Synthesis and Chiral Resolution of Twisted Carbon Nanobelts

Wei Fan,[†,+] Taisuke Matsuno,[‡,+] Yi Han,[†] Xuhui Wang,[†] Qifeng Zhou,[†,§] Hiroyuki Isobe,[,‡] Jishan Wu*[,†,§]*

[†]Department of Chemistry, National University of Singapore, 3 Science Drive 3, 117543, Singapore

[‡]Department of Chemistry, The University of Tokyo, Hongo, Bunkyo-ku, Tokyo 113-0033, Japan

[§]Joint School of National University of Singapore and Tianjin University, International Campus of Tianjin University, Bin-hai New City, Fuzhou 350207, China

[+]These authors contributed equally to this work

Table of Contents

1. Experimental Section

1.1 General information

The starting material **3** was obtained from commercial suppliers and used without further purification. Compounds **2**[1] and **4**[2] were synthesized according to previous literatures. ^{1}H NMR and ^{13}C NMR spectra were recorded in deuterated solvents on a Bruker AVANCE 400 NMR Spectrometer and a Bruker AVIII 500WB NMR Spectrometer. ^{1}H NMR chemical shifts are reported in ppm using the residual protonated solvent as an internal standard and tetramethylsilane (TMS) as reference. High resolution mass spectroscopic measurements were performed on IonSpec 4.7 Tesla Fourier Transform Mass Spectrometer (MALDI-TOF). UV-vis-NIR absorption spectra were recorded on a Shimadzu UV-3600 spectrophotometer. The absolute quantum yields were recorded on a JASCO model FP-6600 spectrofluorometer, equipped with integrating sphere. Time-resolved fluorescence spectroscopic measurements were conducted on a Hamamatsu model compact fluorescence lifetime spectrometer C11367 (Quantaurus-Tau). Cyclic voltammetry (CV) measurements were performed with a Zahner IM6e electrochemical workstation using glassy carbon disc as the working electrode, Pt wire as the counter electrode, Ag/AgCl electrode as the reference electrode. The solution of 0.1 M tetrabutylammonium hexafluorophosphate ($TBAPF_6$) dissolved in chlorobenzene was employed as the supporting electrolyte. Ferrocene was used as an external reference. The analytical HPLC was performed at 40 °C in a column oven (JASCO CO2060PLUS) under detection of UV-vis absorption (JASCO MD2018PLUS) and circular dichromism (CD) intensities (JASCO CD2095PLUS) with a flow rate of 1.0 mL/min. The preparative HPLC was performed at ambient temperature under detection of UV-vis (JASCO UV2075PLUS) with a flow rate of 10 mL/min. CD spectra were obtained on JASCO J-1500.

1.2 Synthetic procedures and characterization data for all new compounds

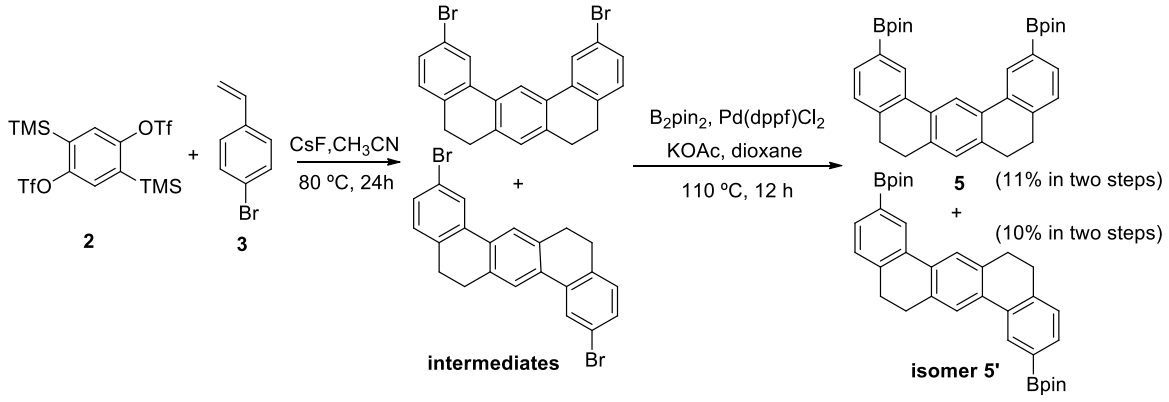

Compound 5:

Compound **2** (6.0 g, 11.4 mmol), compound **3** (10.04 g, 57 mmol) and CsF (10.8 g, 71.16 mmol) were dissolved in dry acetonitrile (130 mL) under N_2 atmosphere. The reaction mixture was heated for

24 h at 110 °C. After cooling to room temperature, solvent was removed under reduced pressure and the residue was extracted by DCM and water. The combined organic layers were dried over $MgSO_4$. After removal of the solvent under vacuum, the residue was purified by silica gel chromatography (Hexane) to afford the intermediate isomers as a white solid (1.8 g). The intermediates were conducted to next step without further purification due to the low solubility.

The intermediates with bis(pinacolato)diboron (4.15 g, 16.36 mmol), Pd(dppf)Cl_2 (117.1 mg, 0.16 mmol) and KOAc (803.1 mg, 8.18 mmol) were dissolved in dry dioxane (40 mL) in a sealed tube with stirrer bar. The reaction mixture was heated for 12 h at 110 °C under N_2 atmosphere. After cooling to room temperature, solvent was removed under reduced pressure and the residue was quickly purified via silica gel column chromatography (DCM). The crude product was and then further purified by preparative GPC using $CHCl_3$ at a rate of 14 mL/min to afford compound **5** (670 mg, 11% in two steps) and isomer **5'** (609 mg, 10% in two steps) as white solid. Compound **5**: ^{1}H NMR (400 MHz, 298 K, CD_2Cl_2): δ ppm 8.28 (s, 2H), 8.25 (s, 1H), 7.61 (dd, ^3J = 5.9 Hz, ^4J = 0.9 Hz, 2H), 7.25 (d, J = 5.9 Hz, 2H), 7.11 (s, 1H), 2.90-2.83 (m, 8H), 1.36 (s, 24H). ^{13}C NMR (100 MHz, $CDCl_3$): δ ppm 140.7, 136.8, 133.9, 133.5, 133.1, 129.9, 127.8, 127.6, 119.2, 83.8, 29.4, 28.6, 24.8, 24.7. Compound **5'**: ^{1}H NMR (400 MHz, 298 K, CD_2Cl_2): δ ppm 8.16 (s, 2H), 7.17 (s, 2H), 7.61 (dd, ^3J = 7.4 Hz, ^4J = 1.1 Hz, 2H), 7.25 (d, J = 7.4 Hz, 2H), 2.91 (s, 8H), 1.34 (s, 24H). ^{13}C NMR (100 MHz, $CDCl_3$): δ ppm 140.9, 136.0, 133.7, 133.4, 129.7, 127.7, 123.4, 83.8, 29.5, 28.7, 24.7. Compound **5**: HRMS analysis (MALDI, 100%, *m*/*z*) calcd for $C_{34}H_{40}B_2O_4$: 534.3119, found 534.3109 (error: -0.3 ppm).

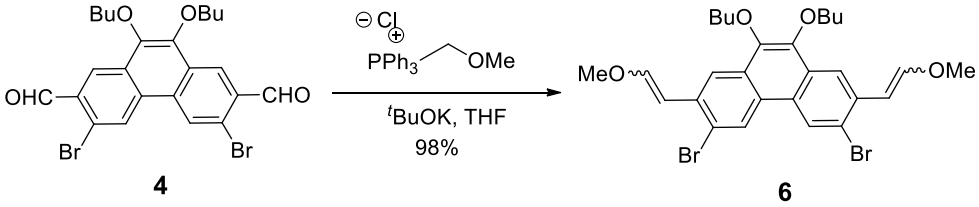

Compound 6:

To a solution of methoxymethyltriphenylphosphonium chloride (767 mg, 2.24 mmol) in dry THF (20 mL) was added ^{t}BuOK (251 mg, 2.24 mmol) at 0 °C under N_2 atmosphere. After stirring for 30 mins, a solution of compound **4** (400 mg, 0.75 mmol) in THF (20 mL) was added and the mixture was stirred at room temperature for 12 h. The reaction was quenched with water and extracted with DCM. The combined organic layers were washed with water and dried over $MgSO_4$. After removal of the solvent under vacuum, the residue was purified by silica gel chromatography (Hexane:DCM = 3:1) to afford compound **6** with two isomers (434 mg, 98%) as a white solid. The *cis*-/*trans*- vinyl isomers could not be separated by silica gel chromatography but did not affect the next reaction. Compound **6**: ^{1}H NMR (400 MHz, 298 K, CD_2Cl_2): δ ppm 8.68 (br, 0.66H), 8.62 and 8.61 (s, 2H), 8.13 and 8.12 (s, 1.25H), 7.15 (d, J = 12.7 Hz, 1.25H), 6.40 (d, J = 7.2 Hz, 0.75H), 6.23 (d, J = 12.8 Hz, 1.25H), 5.75 (d, J = 7.2 Hz, 0.75H),

4.20-4.14 (m, 4H), 3.87 (s, 2.2H), 3.77 (s, 3.8H). 1.91-1.82 (m, 4H), 1.68-1.54 (m, 4H), 1.04-0.99 (m, 4H), ^{13}C NMR (100 MHz, CD_2Cl_2): δ ppm 151.1, 150.2, 143.3, 134.0, 135.0, 133.4, 129.2, 129.1, 128.8, 126.7, 126.6, 126.5, 126.4, 126.2, 126.1, 123.4, 121.6, 121.5, 121.3, 118.3, 104.4, 104.4, 103.3, 103.2, 73.3, 73.3, 61.1, 56.8, 32.6, 32.5, 32.5, 19.5, 13.8, 13.7. Compound **6**: HRMS analysis (MALDI, 100%, *m*/*z*) calcd for $C_{28}H_{32}Br_2O_4$: 590.0662, found 590.0661 (error: -0.1 ppm).

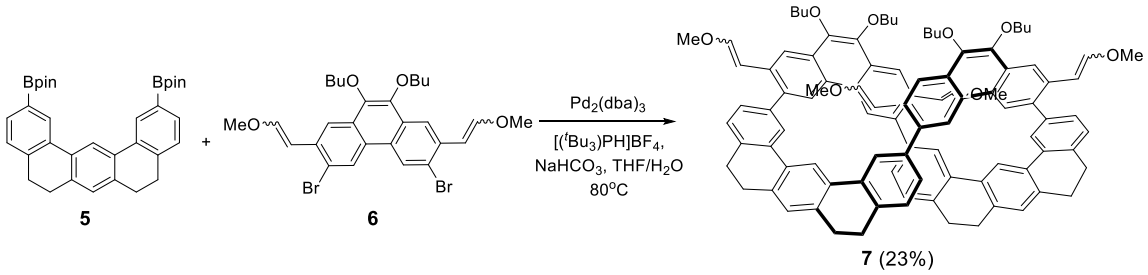

Compound 6:

A mixture of **5** (300 mg, 0.56 mmol), **6** (332.6 mg, 0.56 mmol), $NaHCO_3$ (3.77 g, 44.9 mmol), THF (400 mL) and H_2O (20 mL) was carefully degassed before $Pd_2(dba)_3$ (51.3 mg, 0.056 mmol) and [(*t*-Bu)$_3$PH]BF_4 (65.2 mg, 0.225 mmol) were added. The mixture was stirred and heated at 80 °C for 3 days under N_2 atmosphere. The organic solvent was removed under reduced pressure, then H_2O and DCM were added. The organic layer was separated, dried over anhydrous sodium sulfate. The solvent was removed under vacuum and the residue was first purified by a short column chromatography (silica gel, DCM/Hexane = 1:1) to remove catalysts, and then further purified by preparative GPC using $CHCl_3$ at a rate of 14 mL/min to afford compound **7** (90 mg, 23%) as white solid. The NMR spectrum of **7** is complicated due to existence of multiple *cis*-/*trans*- vinyl isomers. Compound **7**: HRMS analysis (MALDI, 100%, *m*/*z*) calcd for $C_{100}H_{96}O_8$: 1424.7100, found 1424.7100 (error: 0.1 ppm).

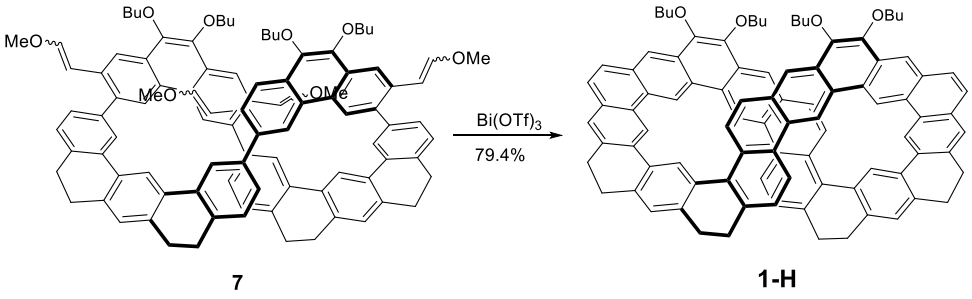

Compound 1-H:

A mixture of **7** (90 mg, 0.063 mmol) and $Bi(OTf)_3$ (8.3 mg, 0.013 mmol) in 1,2-dichloroethane (DCE, 40 mL) was heated at 60 °C for 2 hours under N_2 atmosphere. The organic solvent was removed under reduced pressure, then H_2O and DCM were added. The organic layer was separated, dried over anhydrous sodium sulfate. The solvent was removed and the residue was purified by silica gel chromatography (Hexane:DCM = 3:1) to afford pure compound **1-H** (65 mg, 79%) as a yellow solid. ^{1}H NMR (500 MHz,

298 K, CD_2Cl_2): δ ppm 9.67 (s, 2H), 9.61 (s, 2H), 8.89 (s, 2H), 8.55 (s, 2H), 8.45 (d, *J* = 8.2 Hz, 2H), 8.27 (s, 2H), 8.13 (s, 2H), 8.09 (d, *J* = 9.2 Hz, 2H), 7.88 (d, *J* = 8.9 Hz, 2H), 7.86 (s, 2H), 7.78 (d, *J* = 9.0 Hz, 2H), 7.50 (d, *J* = 9.2 Hz, 2H), 7.46 (d, *J* = 8.2 Hz, 2H), 7.42 (s, 2H), 4.32-4.27 (m, 2H), 4.23-4.17 (m, 4H), 4.09-4.04 (m, 2H), 3.25-2.90 (m, 16H), 1.94-1.88 (m, 4H), 1.81-1.75 (m, 4H), 1.65-1.58 (m, 4H), 1.51-1.44 (m, 4H), 1.01 (t, *J* = 7.4 Hz, 6H), 0.88 (t, *J* = 7.4 Hz, 6H). ^{13}C NMR (125 MHz, 298 K, CD_2Cl_2): δ ppm 142.6, 139.6, 137.6, 137.4, 137.1, 134.1, 133.5, 133.3, 131.6, 130.9, 130.0, 129.0, 128.2, 127.6, 126.9, 126.7, 126.7, 126.5, 126.4, 125.8, 125.4, 123.1, 120.4, 119.7, 119.1, 118.8, 118.6, 73.1, 73.1, 32.6, 32.4, 29.7, 29.1, 28.9, 28.6, 19.5, 19.3, 13.8, 13.6. Compound **1-H**: HRMS analysis (MALDI, 100%, *m*/*z*) calcd for $C_{96}H_{80}O_4$: 1296.6051, found 1296.6047 (error: 0.3 ppm).

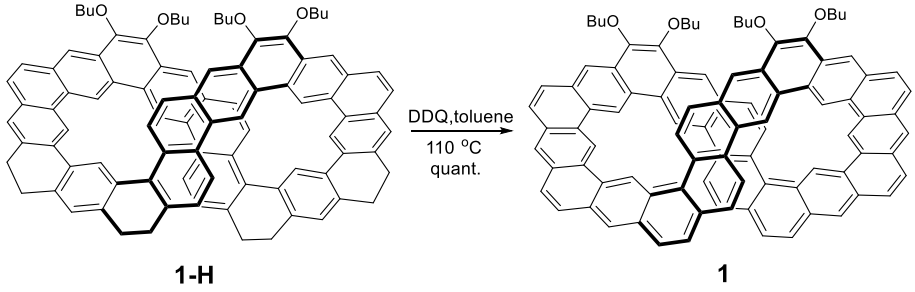

1-H **1**

Compound 1:

A mixture of **1-H** (91 mg, 0.07 mmol) and DDQ (191 mg, 0.84 mmol) in dry toluene was heated at 110 °C for 24 hours under N_2 atmosphere. The organic solvent was removed under reduced pressure, then H_2O and DCM were added. The organic layer was separated, dried over anhydrous sodium sulfate. The solvent was removed and the crude was washed by methanol and acetonitrile to afford pure compound **1** as yellow solid (90 mg, quantitative). ^{1}H NMR (500 MHz, 373 K, toluene-d_8): δ ppm 10.11 (s, 2H), 10.09 (s, 2H), 9.83 (s, 2H), 9.26 (s, 2H), 8.71 (s, 2H), 8.37 (d, *J* = 9.1 Hz, 2H), 8.17 (s, 2H), 8.16 (s, 2H), 7.92 (d, *J* = 8.3 Hz, 2H), 7.87 (s, 2H), 7.84 (d, *J* = 9.0 Hz, 2H), 7.78 (d, *J* = 9.1 Hz, 2H), 7.75 (d, *J* = 9.2 Hz, 2H), 7.84 (d, *J* = 9.0 Hz, 2H), 7.68 (d, *J* = 9.0 Hz, 8H), 7.46 (d, *J* = 8.2 Hz, 2H), 7.28 (d, *J* = 8.4 Hz, 2H), 7.25 (d, *J* = 9.1 Hz, 2H), 6.91 (d, *J* = 8.3 Hz, 2H), 4.44-4.40 (m, 2H), 4.38-4.33 (m, 2H), 4.30-4.26 (m, 2H), 4.20-4.16 (m, 2H), 2.03-1.97 (m, 2H), 1.87-1.81 (m, 2H), 1.72-1.65 (m, 2H), 1.57-1.50 (m, 2H), 1.07 (t, *J* = 7.4 Hz, 6H), 0.93 (t, *J* = 7.4 Hz, 6H). ^{13}C NMR (125 MHz, THF-d_8,): δ ppm 143.7, 143.6, 132.1, 131.9, 131.6, 131.3, 131.4, 130.3, 130.1, 130.0, 129.6, 129.2, 129.2, 129.0, 129.0, 128.8, 128.4, 127.9, 127.5, 127.5, 127.4, 127.2, 127.1, 126.9, 126.4, 126.0, 126.0, 125.6, 124.8, 121.7, 121.2, 121.0, 120.5, 120.0, 73.6, 33.4, 33.2, 30.4, 25.4, 25.3, 25.1, 25.0, 24.8, 20.2, 20.1, 14.2, 14.1. Compound **1**: HRMS analysis (MALDI, 100%, *m*/*z*) calcd for $C_{96}H_{72}O_4$: 1288.5425, found 1288.5415 (error: -0.8 ppm).

2. Additional spectra for characterizations of 1-H and 1

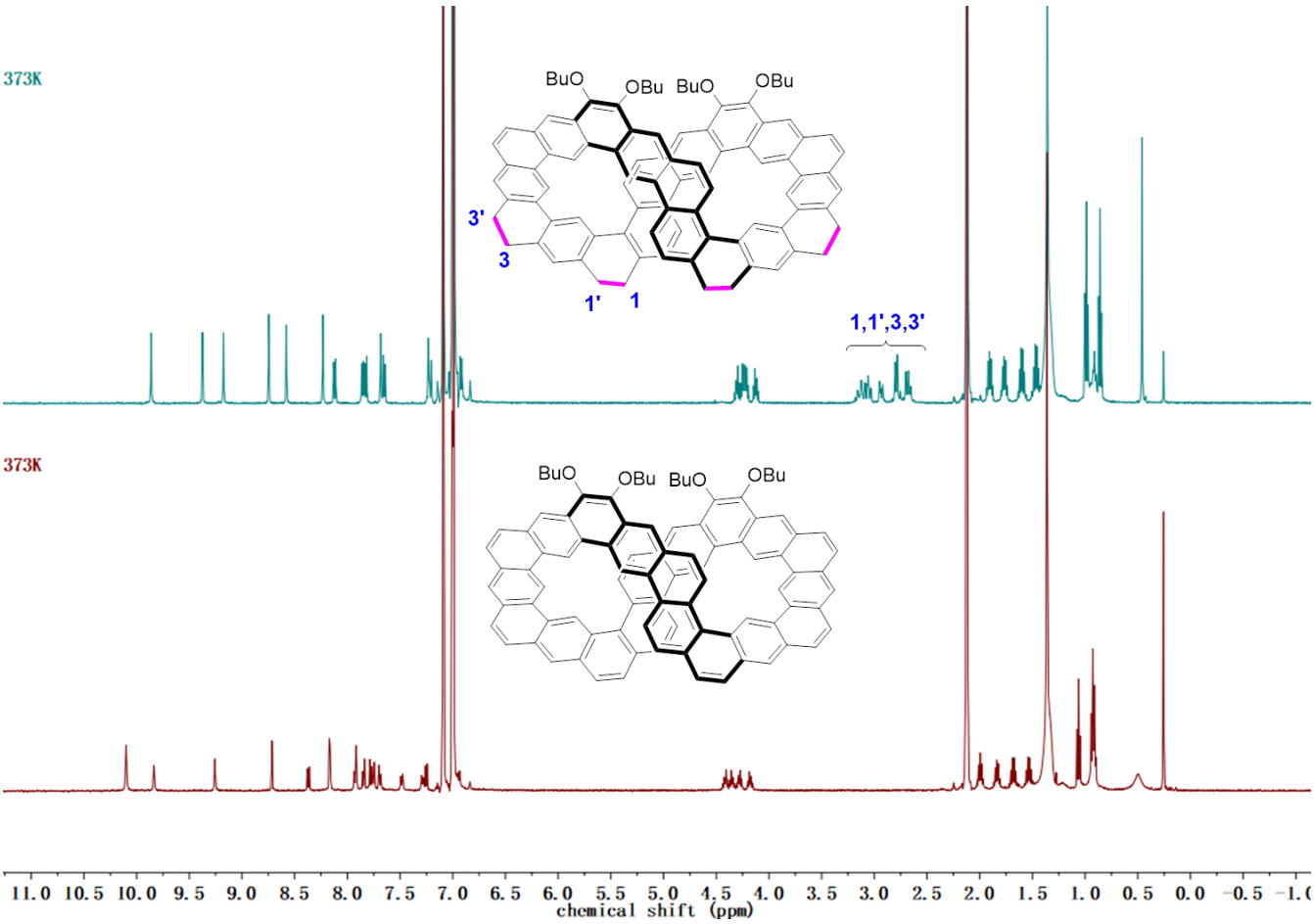

Figure S1. The full rang ^{1}H NMR spectra of **1-H** (top) and **1**(down) in toluene-d_8 (500 MHz) at 373K. The multiple split peaks of 1, 1', 3, 3' on the saturated sp^3 carbons at 2.1~3.2 ppm in **1-H** disappear after dehydrogenation to afford **1**.

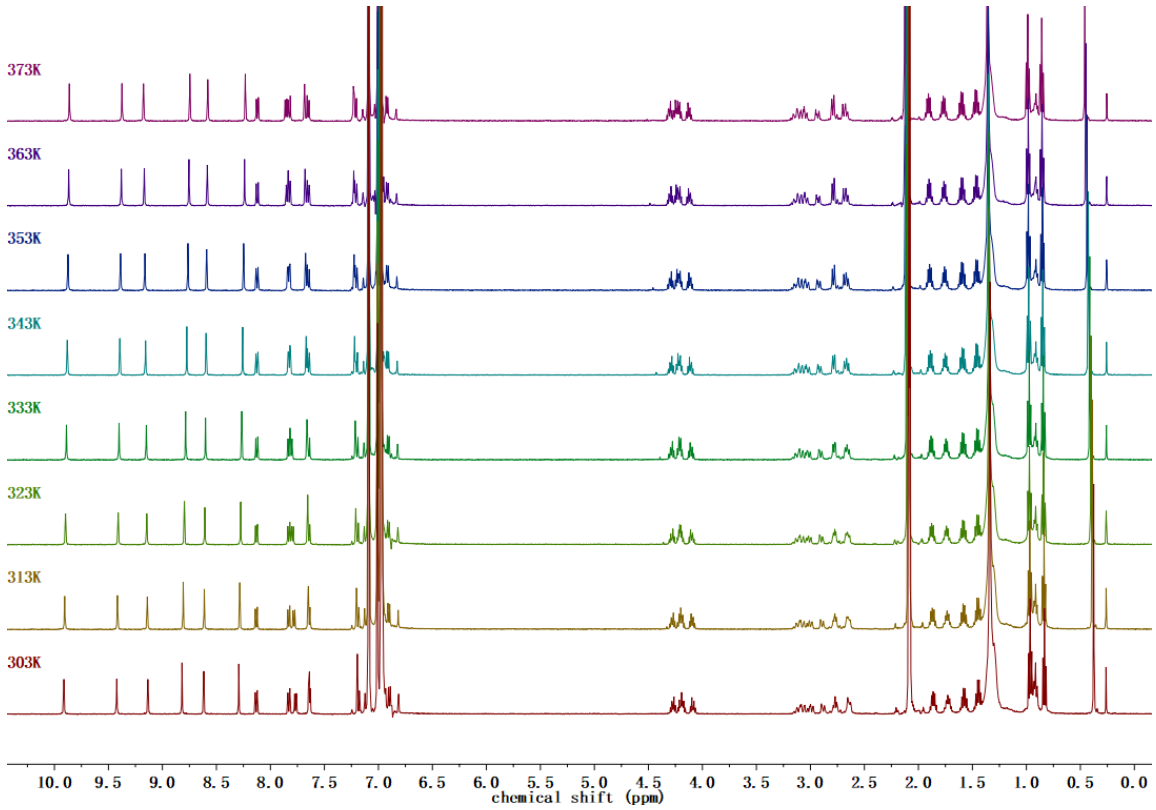

Figure S2. VT ^{1}H NMR spectra of **1-H** in toluene-d_8 (500 MHz).

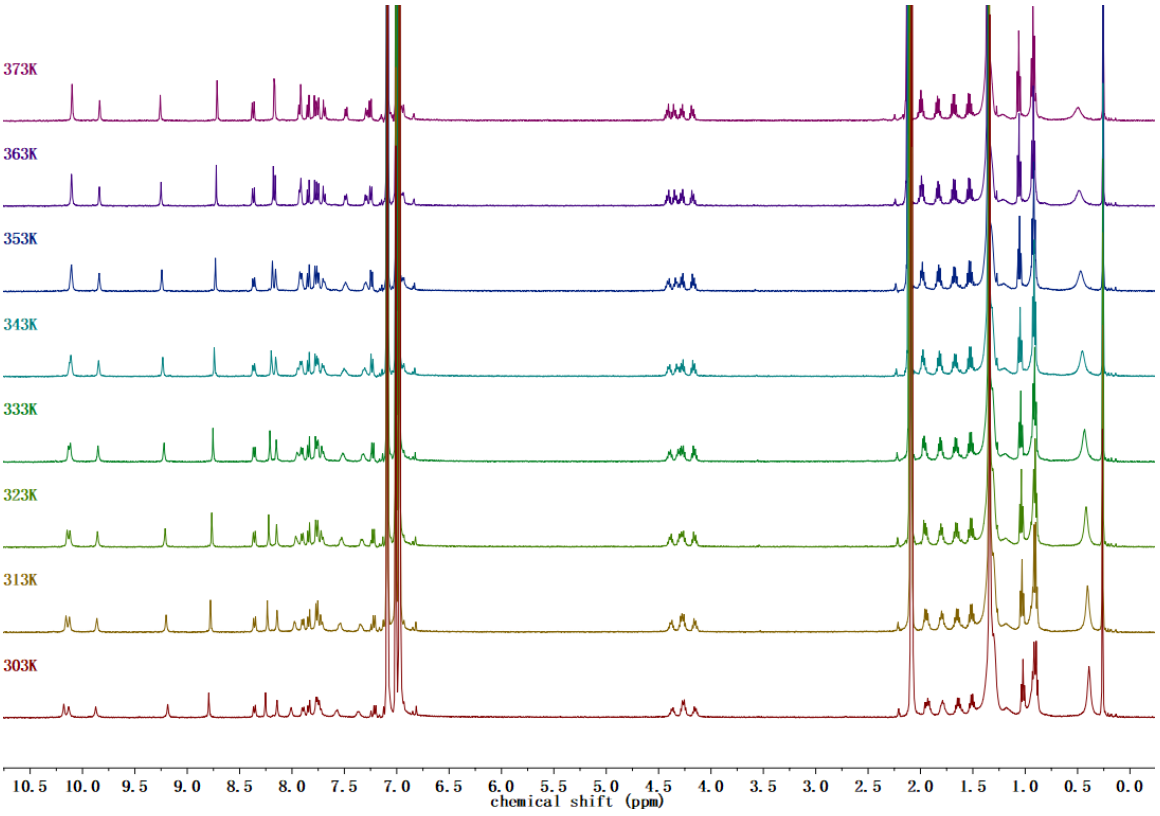

Figure S3. VT ^{1}H NMR spectra of **1** in toluene-d_8 (500 MHz).

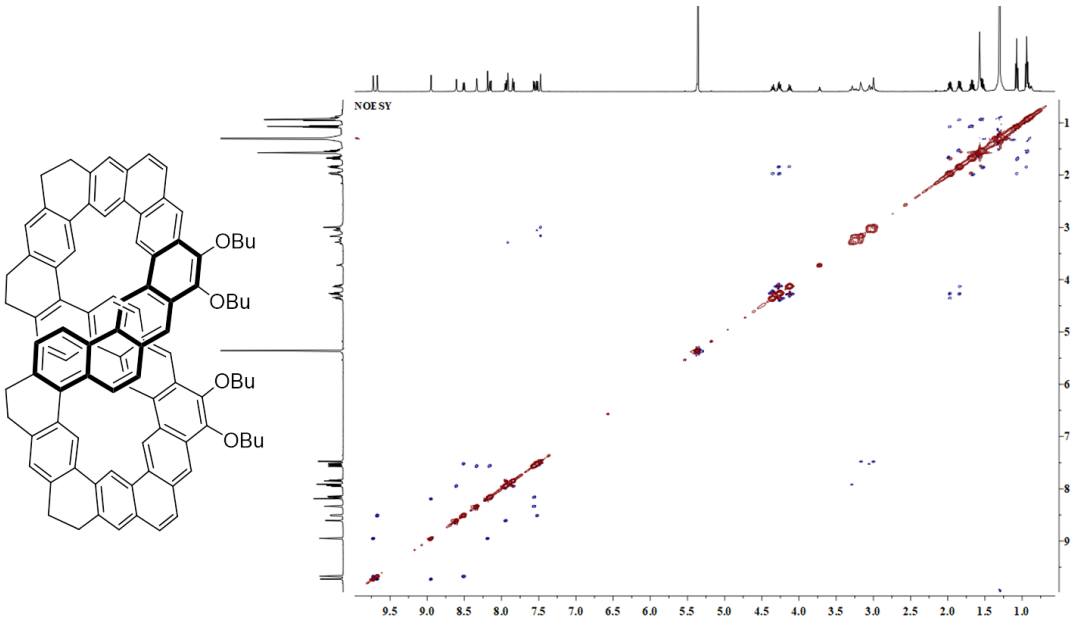

Figure S4. 2D NOESY NMR spectrum of **1-H** in CD_2Cl_2 (500 MHz) at 298 K showing correlations.

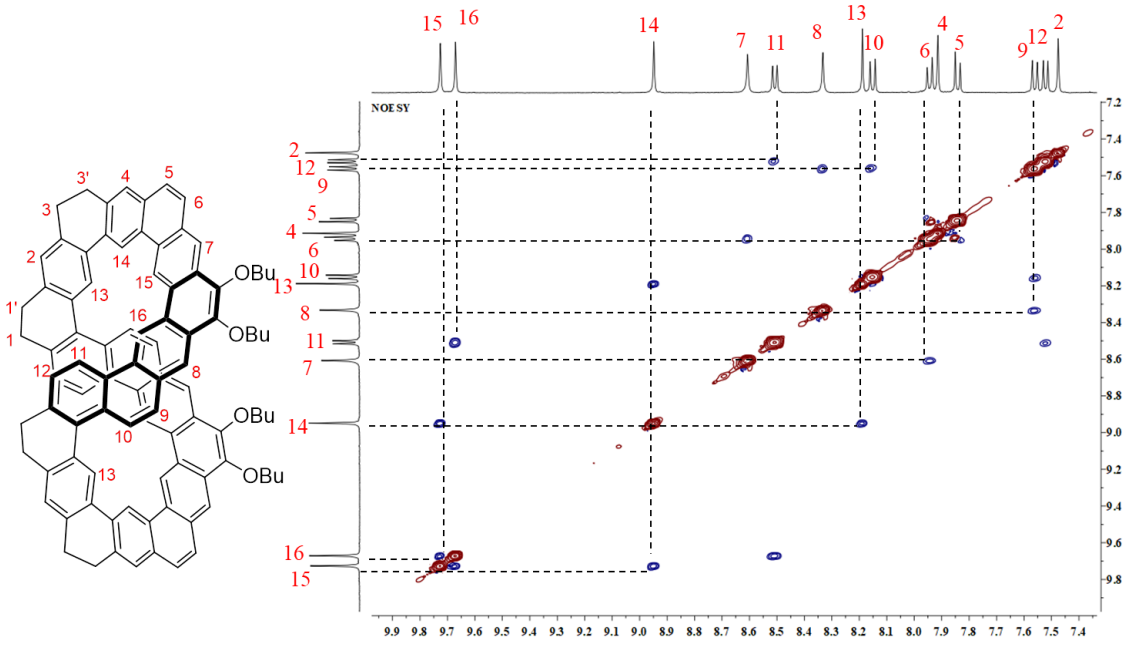

Figure S5. Partial 2D NOESY NMR spectrum of **1-H** in CD_2Cl_2 (500 MHz) at 298 K showing aromatic/aromatic correlations.

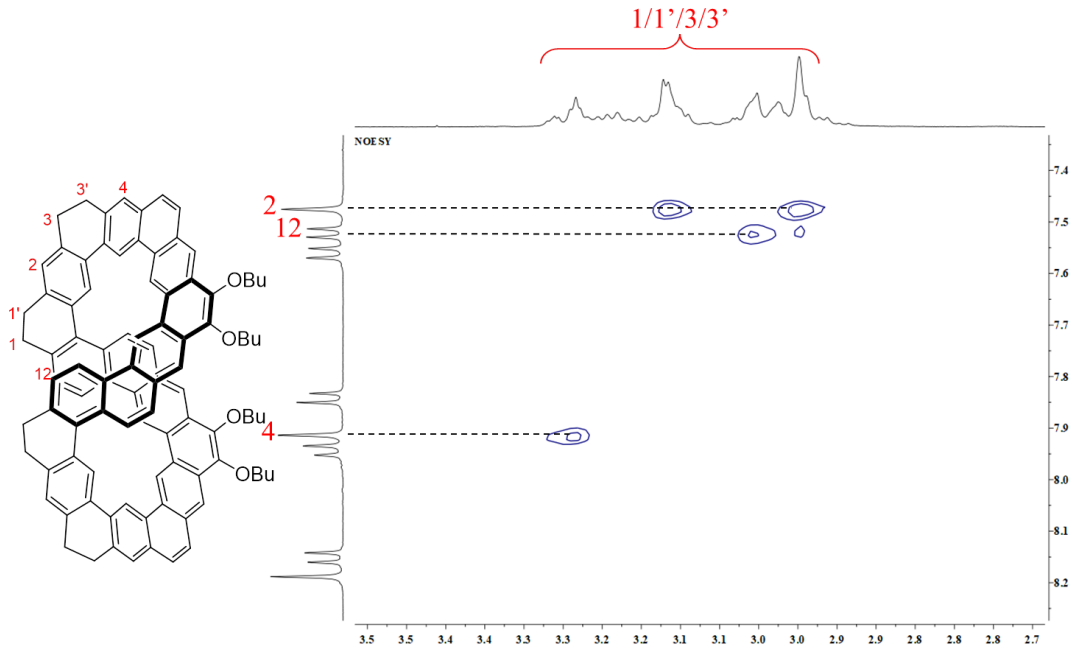

Figure S6. Partial 2D NOESY NMR spectrum of **1-H** in CD_2Cl_2 (500 MHz) at 298 K showing aromatic/aliphatic correlations.

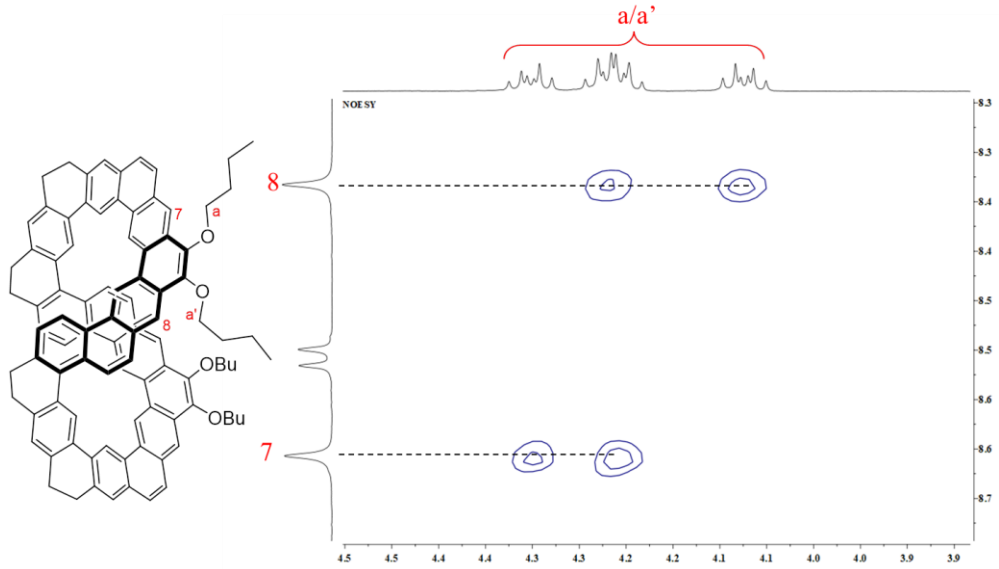

Figure S7. Partial 2D NOESY NMR spectrum of **1-H** in CD_2Cl_2 (500 MHz) at 298 K showing aromatic/aliphatic correlations.

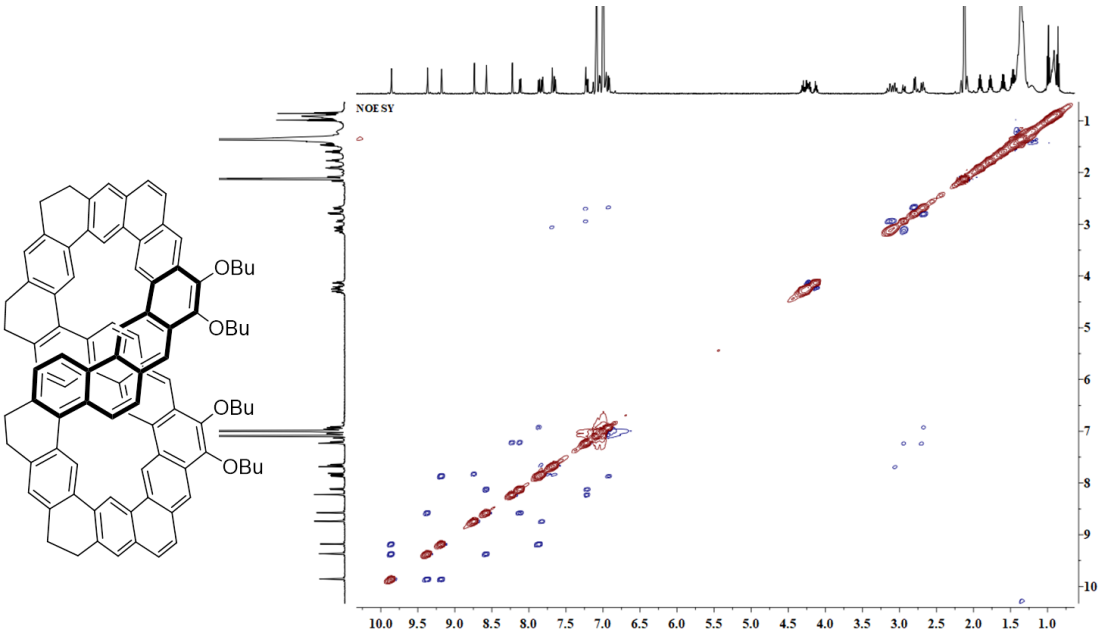

Figure S8. 2D NOESY NMR spectrum of **1-H** in toluene-d_8 (500 MHz) at 373 K showing correlations.

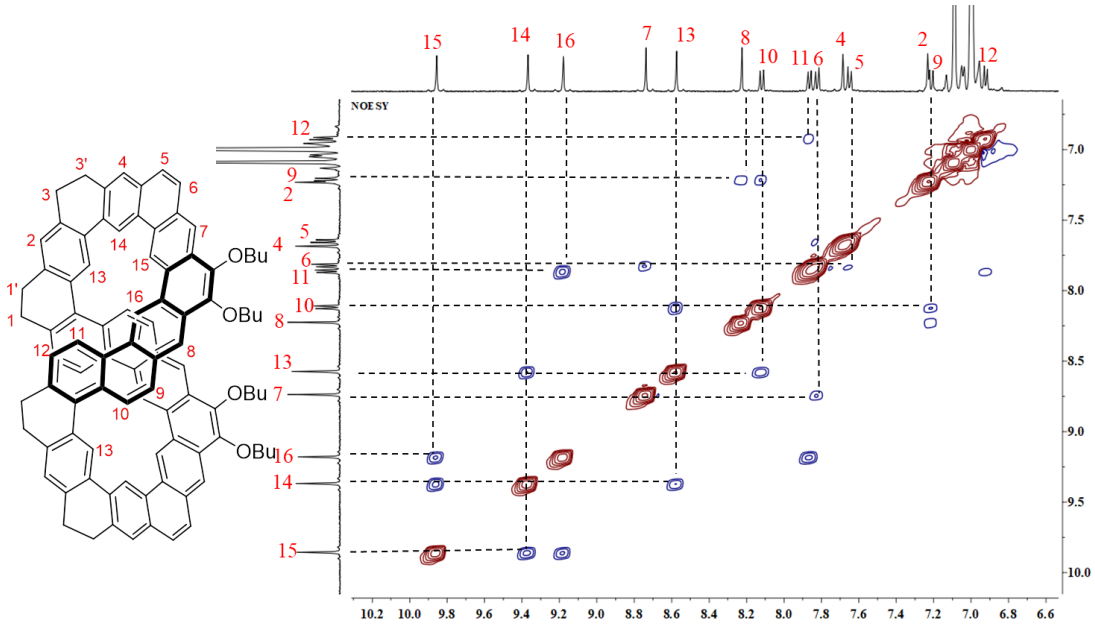

Figure S9. Partial 2D NOESY NMR spectrum of **1-H** in toluene-d_8 (500 MHz) at 373 K showing aromatic/aromatic correlations.

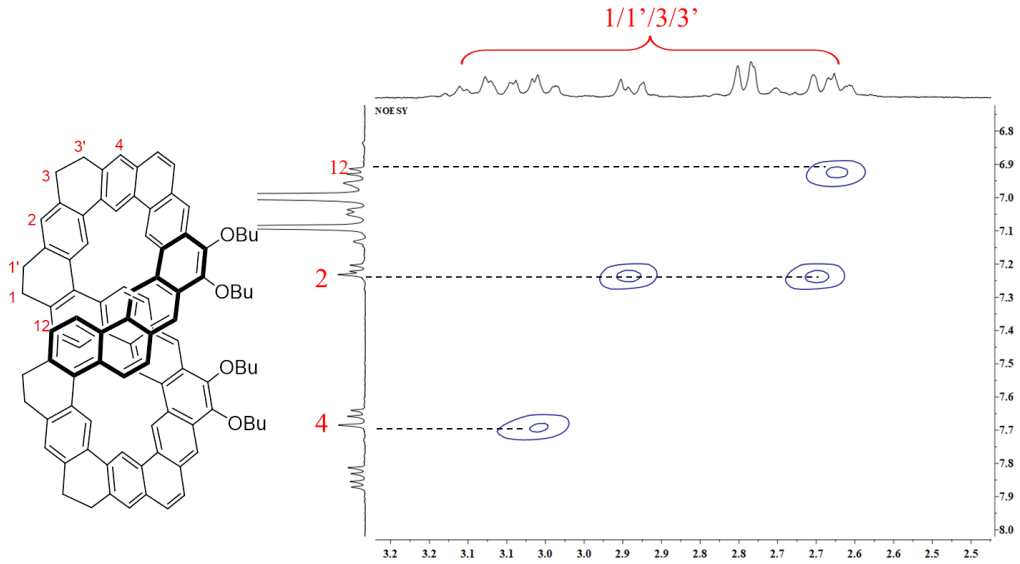

Figure S10. Partial 2D NOESY NMR spectrum of **1-H** in toluene-d_8 (500 MHz) at 373 K showing aromatic/aliphatic correlations.

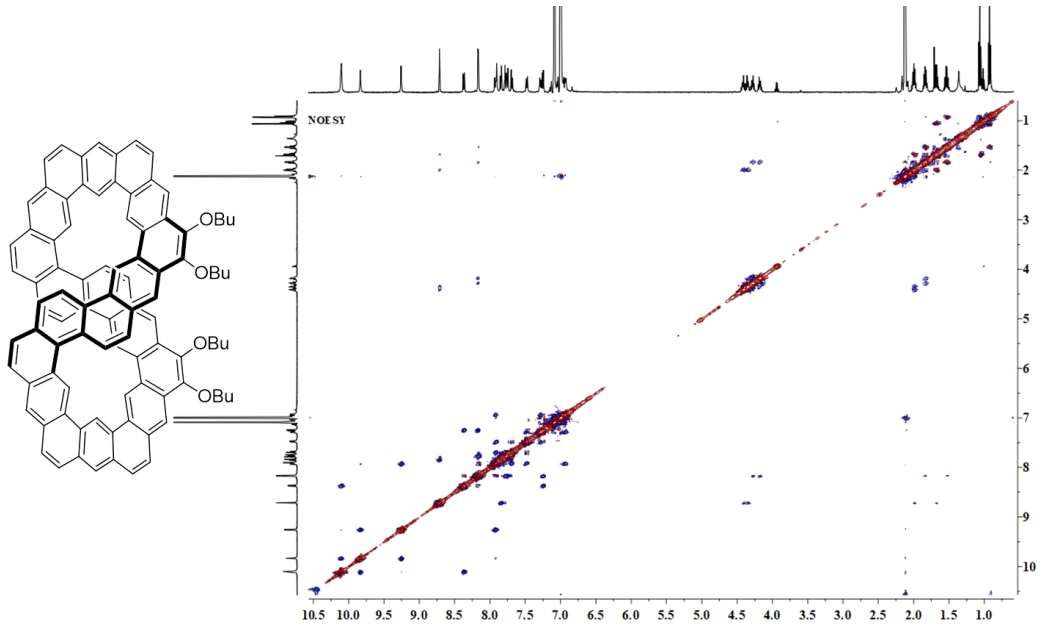

Figure S11. 2D NOESY NMR spectrum of **1** in toluene-d_8 (500 MHz) at 373 K showing correlations.

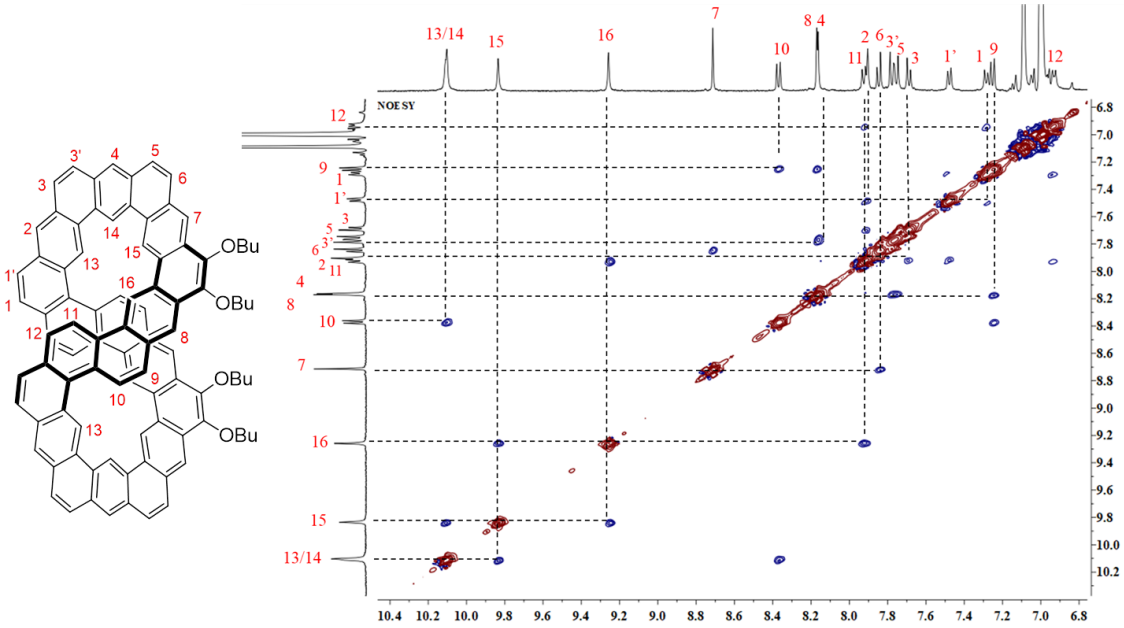

Figure S12. Partial 2D NOESY NMR spectrum of **1** in toluene-d_8 (500 MHz) at 373 K showing aromatic/aromatic correlations.

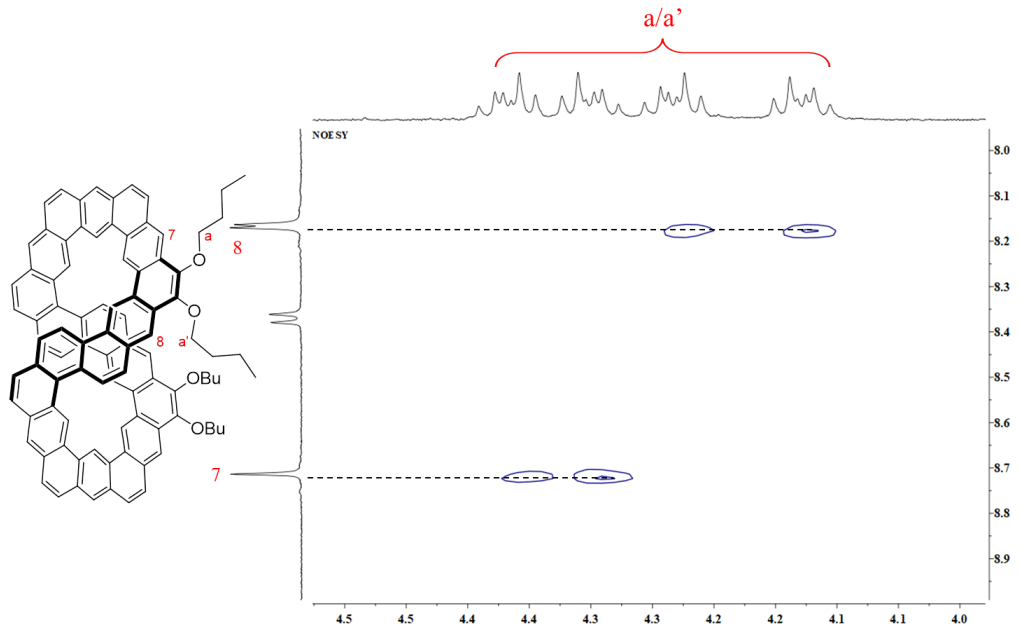

Figure S13. Partial 2D NOESY NMR spectrum of **1** in toluene-d_8 (500 MHz) at 373 K showing aromatic/aliphatic correlations.

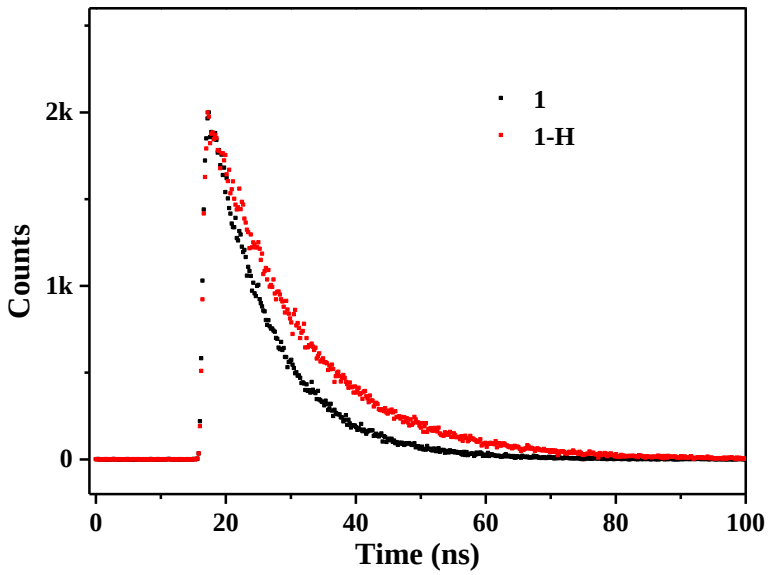

Figure S14. Time-resolved fluorescence decay profiles of **1-H** (λ_{exc} = 340 nm, λ_{probe} = 460 nm) and **1** (λ_{exc} = 365 nm, λ_{probe} = 473 nm).

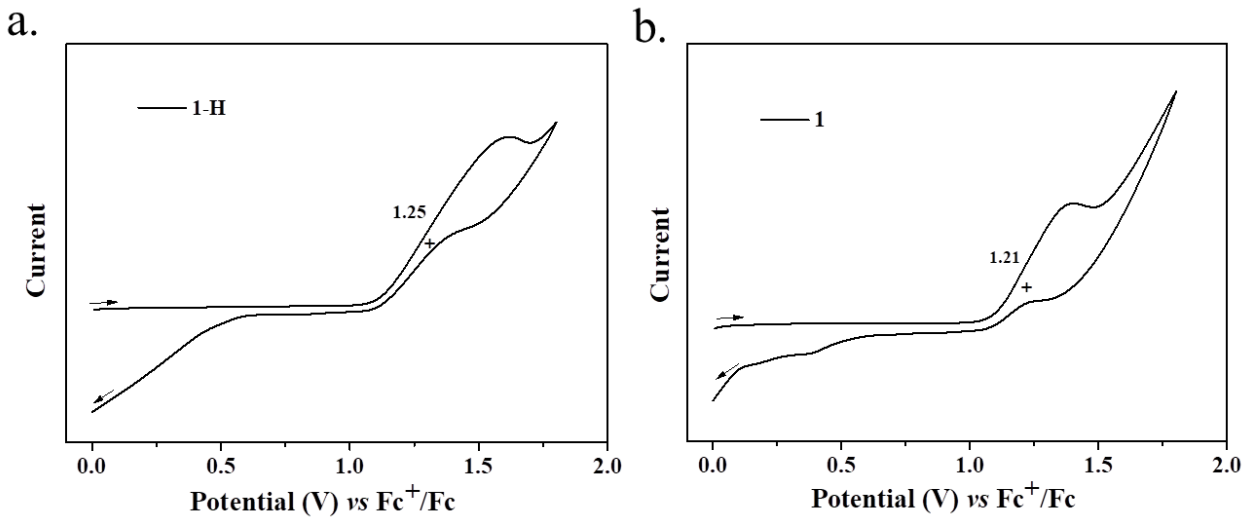

Figure S15. Cyclic voltammogram of (a) **1-H** and (b) **1** measured in chlorobenzene with $TBAPF_6$ as supporting electrolyte. The downward curves at the end of potential flow may arise from the deposition and coupling of the oxidized species on the surface of work electrode after the first scan.

3. Chiral resolution and chiroptic properties for 1-H and 1

3.1 Chiral HPLC analysis and optical resolution of 1-H and 1

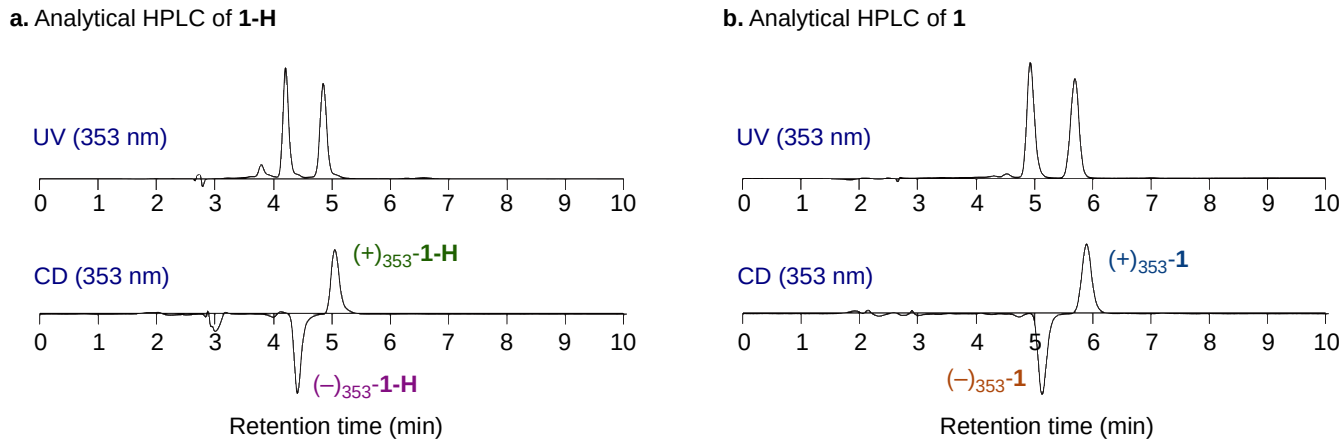

Figure S16. Chiral HPLC analyses of racemic specimens. [Conditions] Column: COSMOSIL Cholester 4.6ϕ × 250 mm, Column oven: 40 °C, UV detector: 353 nm, CD detector: 353 nm, eluent: CH_2Cl_2/MeOH (7:3 v/v), flow rate: 1.0 mL min^{-1}. (a) Chromatograms of (*rac*)-**1-H**. (b) Chromatograms of (*rac*)-**1**.

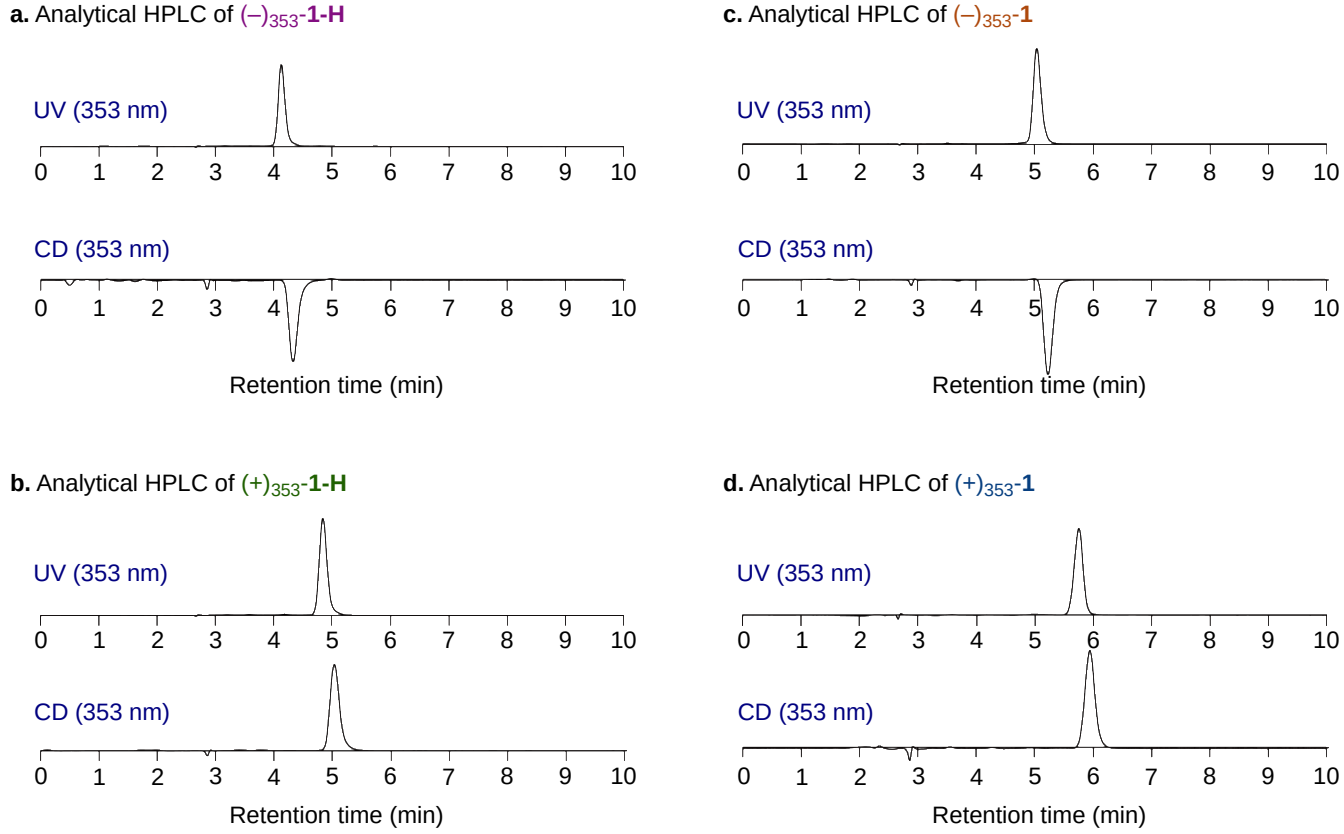

Figure S17. Chiral HPLC analyses of separated enantiomers. [Conditions] Column: COSMOSIL Cholester 4.6ϕ × 250 mm, Column oven: 40 °C, UV detector: 353 nm, CD detector: 353 nm, eluent: CH_2Cl_2/MeOH (7:3 v/v), flow rate: 1.0 mL min^{-1}. (a) Chromatograms of $(–)_{353}$-**1-H**. (b) Chromatograms of $(+)_{353}$-**1-H**. (c) Chromatograms of $(–)_{353}$-**1**. (d) Chromatograms of $(+)_{353}$-**1**.

3.2 UV-vis and CD spectra of 1-H and 1

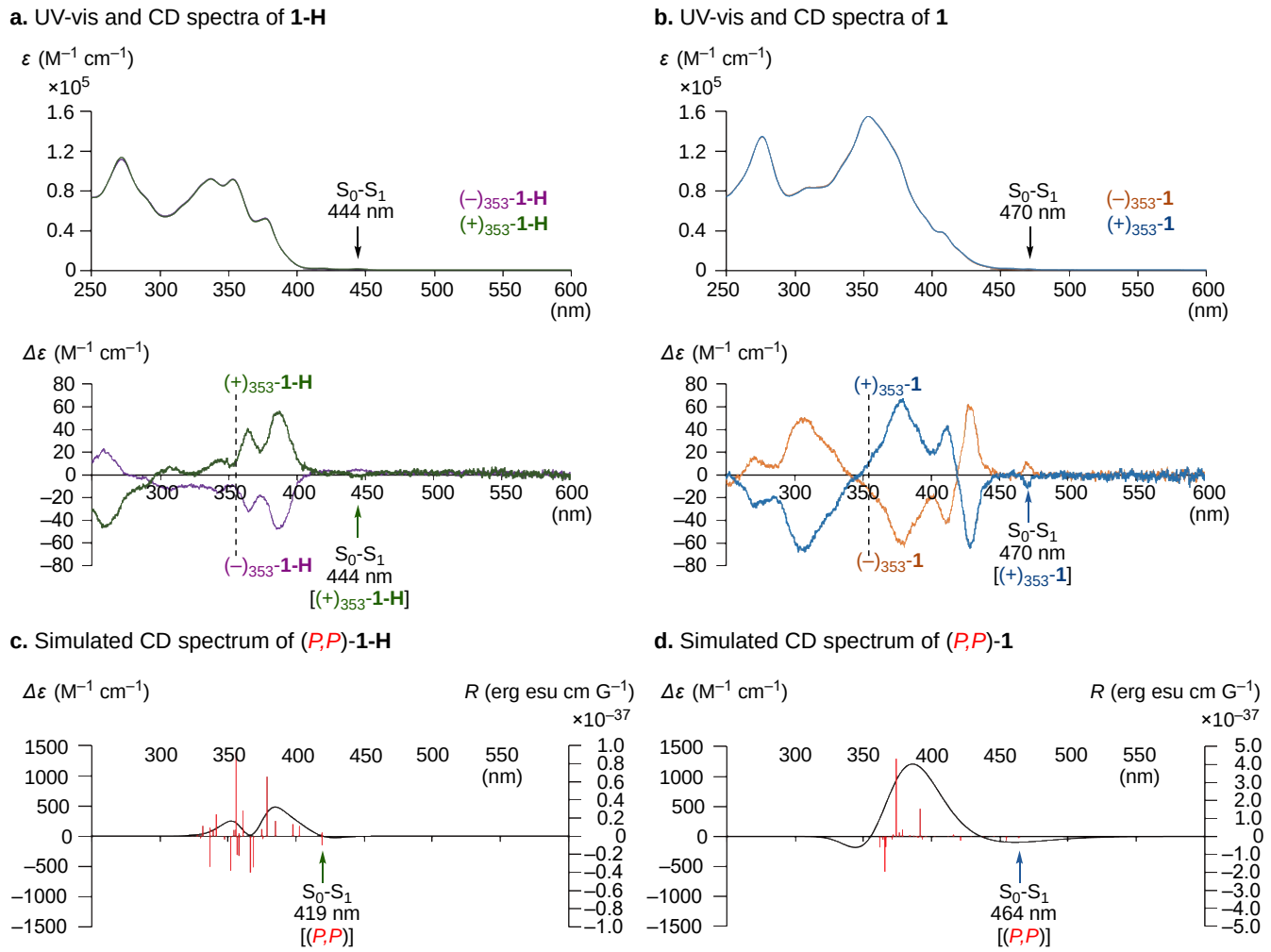

Figure S18. UV-vis absorption and CD spectra in DCM at 298 K and simulation of CD spectra. (a) UV-vis and CD spectra of (–)$_{353}$-**1-H** (1.06×10^{-5} M) and (+)$_{353}$-**1-H** (7.73×10^{-6} M). (b) UV-vis and CD spectra of (–)$_{353}$-**1** (8.99×10^{-6} M) and (+)$_{353}$-**1** (8.70×10^{-6} M). (c) Simulated CD spectra of (*P*,*P*)-**1-H**. The sign of S_0-S_1 transition was minus, which led us to assign (+)$_{353}$-**1-H** as (*P*,*P*)-isomer. (d) Simulated CD spectra of (*P*,*P*)-**1**. The sign of S_0-S_1 transition was minus, which led us to assign (+)$_{353}$-**1-H** as (*P*,*P*)-isomer.

3.3 Measurement of g_{abs} values of 1-H and 1

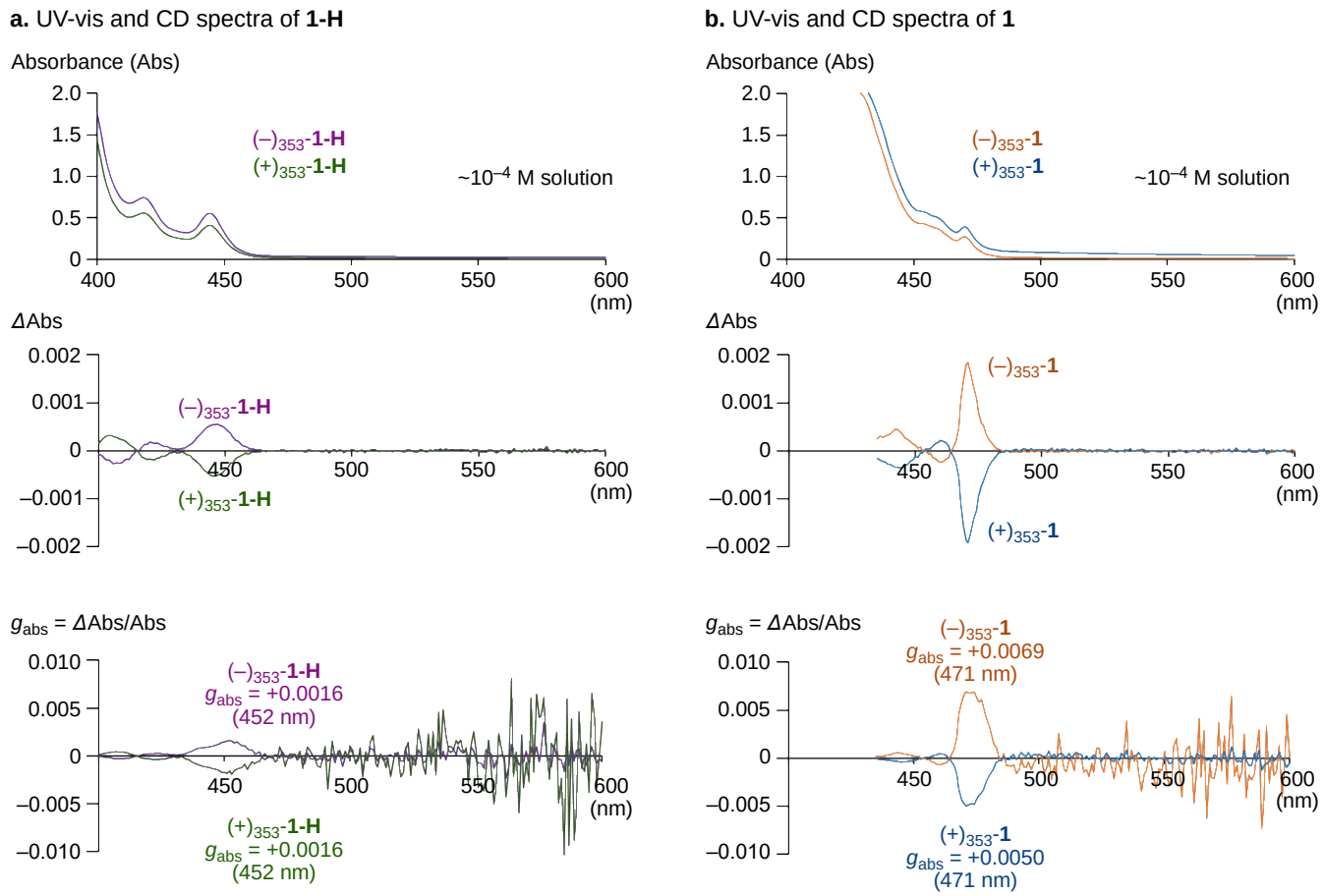

Figure S19. UV-vis absorption and CD spectra in DCM at 298 K. (a) UV-vis and CD spectra of (–)$_{353}$-**1-H** (~10^{-4} M) and (+)$_{353}$-**1-H** (~10^{-4} M). (b) UV-vis and CD spectra of (–)$_{353}$-**1** (~10^{-4} M) and (+)$_{353}$-**1** (~10^{-4} M).

4. DFT calculations for 1-H and 1

Density functional theory (DFT) calculations were performed with the Gaussian09 program suite[3] with Becke's three-parameter hybrid exchange functionals and the Lee-Yang-Parr correlation functional (B3LYP) employing the 6-31G(d,p) basis set for all atoms.[4] Time-dependent DFT (TD-DFT) calculations were performed at the (U)B3LYP/6-31G(d,p) level of theory under vacuum. NICS values were calculated (B3LYP/6-31G(d,p)) using the standard GIAO procedure (NMR pop=NCSall).[5] ACID plot (B3LYP/6-31G(d,p)) was calculated by using the method developed by Herges based on the optimized ground-state geometries.[6] The iso-chemical shielding surface (ICSS)[7] calculations were carried out and the VMD programme[8] was used to plot ICSS cube files.

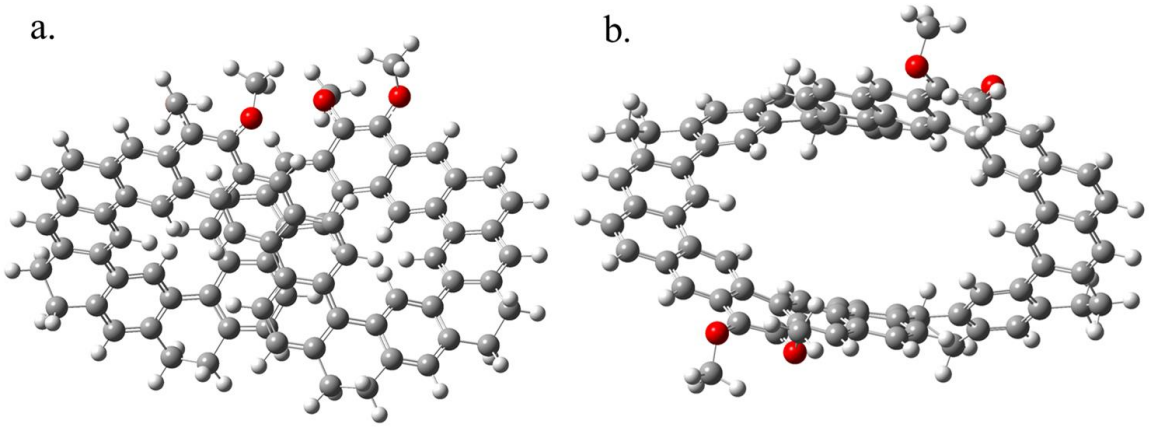

Figure S20. The optimized geometry of **1-H** (left for top-view and right for side-view) at B3LYP/6-31G(d,p) level of theory showing a twisted backbone. The *n*-butoxy substituents are replaced by methoxy groups during the calculations.

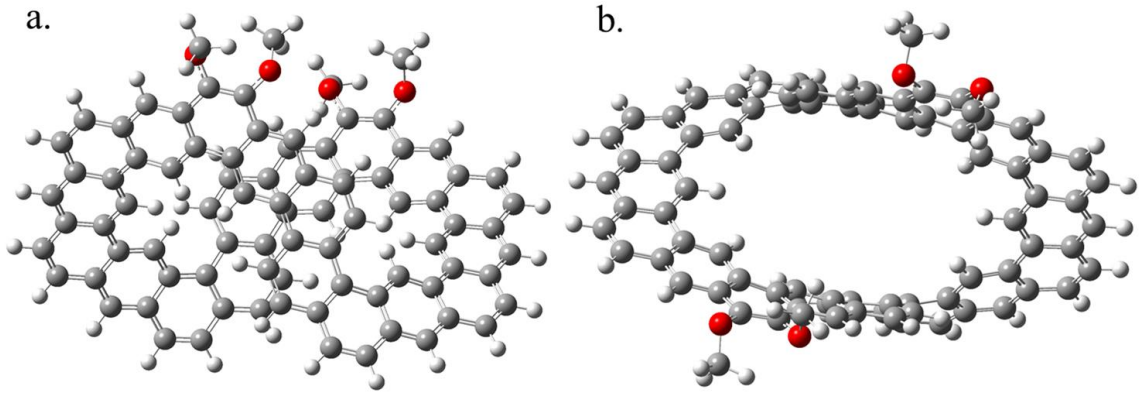

Figure S21. The optimized geometry of **1** (left for top-view and right for side-view) at B3LYP/6-31G(d,p) level of theory showing a twisted backbone. The *n*-butoxy substituents are replaced by methoxy groups during the calculations.

a. Method for **1-H**

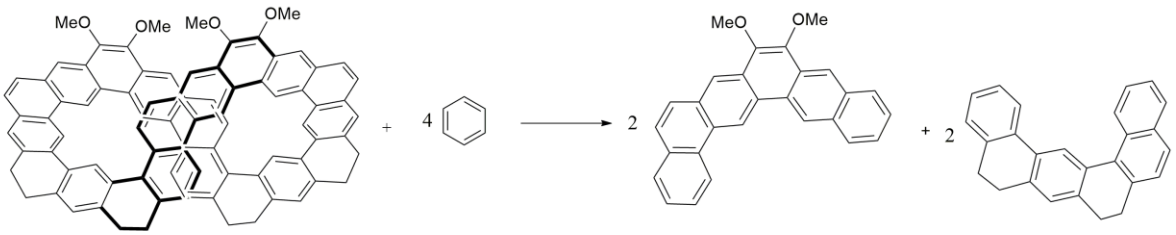

b. Method for **1**

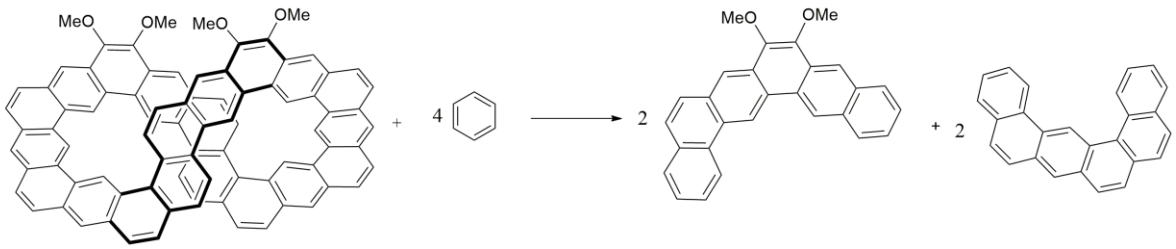

Figure S22. The hypothetical homodesmotic reactions applied in the calculation of strain energy for **1-H** and **1**. The *n*-butoxy substituents are replaced by methoxy groups during the calculations.

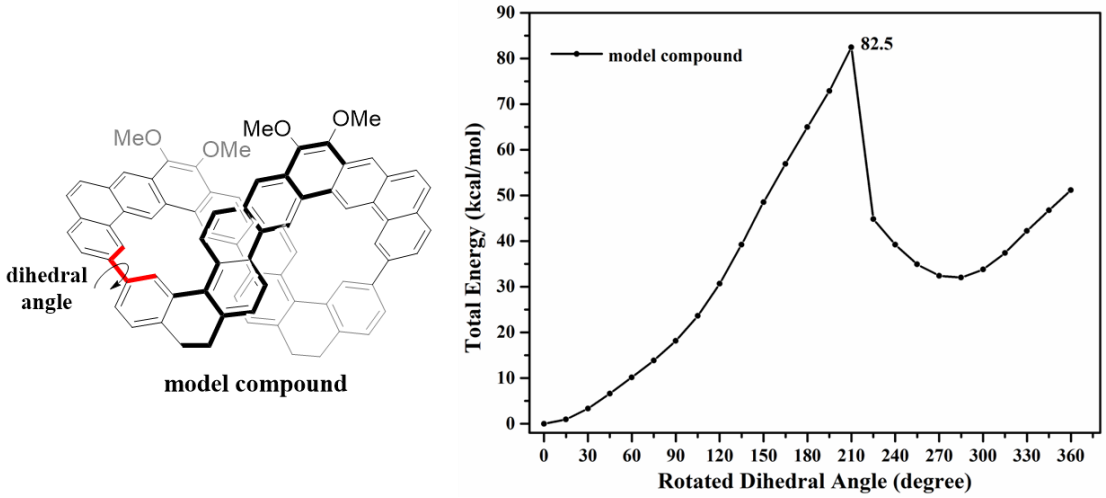

Figure S23. Calculated total energies of an analogue of **1** with a partially fused structure (named as **model compound**) by rotating the dihedral angle (highlight with red). The relatively high energy (up to 82.5 kcal/mol when rotated 210°) indicate a high racemization barrier.

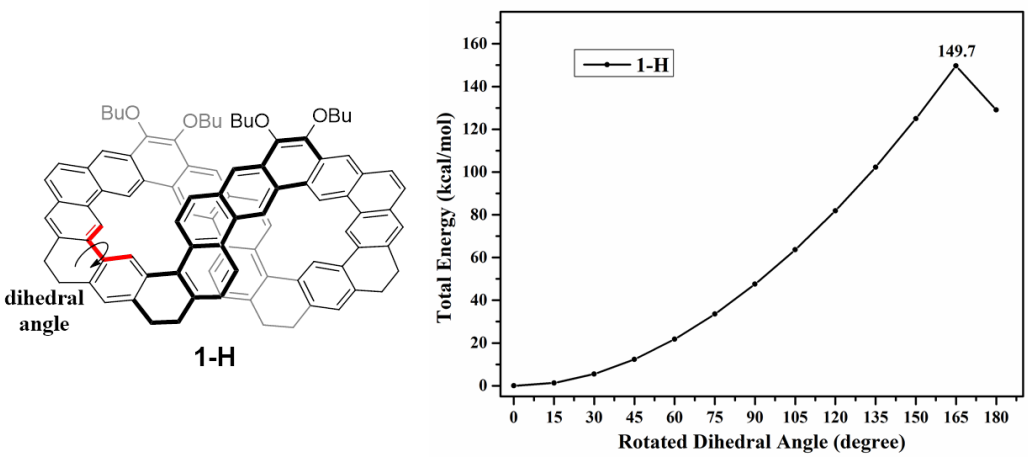

Figure S24. Calculated total energies of **1-H** by rotating the dihedral angle (highlight with red). The very high energy (up to 149.7 kcal/mol when rotated 165°) indicates a very rigid configuration with persistent chirality.

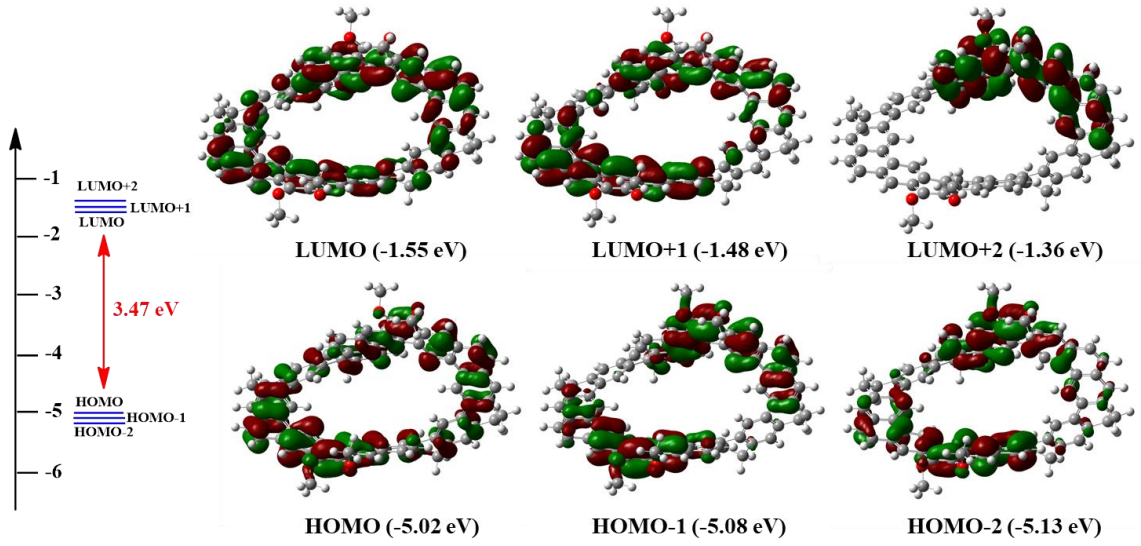

Figure S25. Frontier molecular orbital profiles and energy diagram of **1-H** obtained by B3LYP/6-31G(d,p) level calculation.

Table S1. Selected TD-DFT (B3LYP/6-31G(d,p)) calculated energies, oscillator strength and compositions of major electronic transitions of **1-H**.

Wavelength (nm)	Osc.Strength (f)	Major contributions
420.48495	0.006	H-1->LUMO (31%), HOMO->L+1 (38%)
419.53167	0.0312	H-2->LUMO (16%), H-1->L+1 (26%), HOMO->LUMO (29%)
403.90993	0.0039	H-3->LUMO (37%), H-2->L+1 (26%), HOMO->L+1 (24%)
400.73756	0.1512	H-3->L+1 (10%), H-2->LUMO (20%), HOMO->LUMO (46%)
386.2075	0.0351	H-1->LUMO (39%), HOMO->L+1 (16%)
381.54852	0.0649	H-3->LUMO (11%), H-1->L+1 (16%), H-1->L+3 (15%), HOMO->LUMO (10%), HOMO->L+3 (21%)
380.15635	0.0826	H-3->LUMO (13%), H-1->L+1 (23%), H-1->L+2 (10%), HOMO->L+2 (14%)
376.96623	0.5091	H-2->LUMO (52%), H-1->L+1 (10%)
374.23542	0.1987	H-3->LUMO (24%), H-2->L+1 (41%)
372.70544	0.1765	H-4->L+1 (11%), H-3->L+1 (26%), H-1->L+1 (11%), HOMO->L+2 (16%)
370.14627	0.2217	H-4->LUMO (17%), H-2->L+1 (10%), HOMO->L+2 (13%), HOMO->L+3 (18%)
366.28613	1.0538	H-4->L+1 (22%), H-3->L+1 (39%)
364.38075	0.4371	H-4->LUMO (23%), H-1->L+2 (40%), HOMO->L+2 (13%)
362.97264	0.2613	H-4->LUMO (27%), H-4->L+1 (17%), H-1->L+3 (33%), HOMO->L+3 (11%)
361.2593	0.0581	H-4->LUMO (16%), H-2->L+2 (27%), H-1->L+2 (14%)
359.38489	0.0758	H-4->L+1 (12%), H-3->L+3 (13%), H-2->L+3 (29%), H-1->L+3 (10%)
357.16934	0.0282	H-3->L+2 (55%), H-2->L+2 (21%)
356.30713	0.0141	H-4->L+2 (16%), H-3->L+3 (24%)
354.74733	0.0138	H-4->L+3 (10%), H-3->L+3 (32%), H-2->L+3 (21%)
354.26079	0.0513	H-4->L+1 (17%), H-4->L+2 (20%), H-4->L+3 (13%), H-3->L+3 (11%), H-1->L+4 (16%)
346.64409	0.0266	HOMO->L+4 (80%)
341.75196	0.17	H-5->LUMO (11%), H-4->L+2 (11%), H-4->L+3 (11%), H-3->L+4 (11%), H-1->L+4 (40%)
339.02325	0.0018	H-5->LUMO (36%), HOMO->L+5 (43%)
337.68437	0.0631	H-4->L+2 (19%), H-4->L+3 (17%), H-2->L+4 (39%)
336.43817	0.2532	H-3->L+4 (50%), HOMO->L+5 (11%)
331.46422	0.0209	H-5->LUMO (38%), H-1->L+4 (22%), HOMO->L+5 (18%)
329.06256	0.0029	H-5->L+1 (51%), HOMO->L+7 (13%)
328.18283	0.0577	H-5->L+1 (27%), H-2->L+4 (31%), H-1->L+5 (19%)
326.42882	0.0013	H-3->L+4 (18%), H-2->L+5 (11%), HOMO->L+6 (17%)
322.69903	0.0264	H-2->L+5 (20%), H-1->L+5 (29%)
321.9198	0.0174	H-2->L+5 (35%), H-1->L+5 (21%)
320.55482	0.0274	H-3->L+5 (79%)
319.97572	0.0639	H-5->L+2 (11%), H-5->L+3 (12%), H-4->L+5 (16%), HOMO->L+7 (13%)
319.62927	0.0659	H-6->LUMO (11%), H-5->L+2 (13%), H-5->L+3 (12%), H-2->L+6 (11%), HOMO->L+6 (15%)
317.97341	0.0125	H-4->L+4 (86%)
316.76297	0.0923	H-6->LUMO (26%), H-5->L+2 (28%)
316.02822	0.0162	H-6->L+1 (26%), H-5->L+3 (34%)
315.6983	0.0192	H-4->L+5 (19%), H-2->L+7 (20%), H-1->L+6 (29%)
310.76848	0.1126	H-6->LUMO (36%), H-2->L+6 (14%)
308.98717	0.0161	H-8->LUMO (13%), H-1->L+7 (13%), HOMO->L+6 (36%)
308.61031	0.0159	H-7->LUMO (13%), H-6->L+1 (35%)
306.80044	0.0011	H-4->L+5 (23%), H-1->L+6 (18%), HOMO->L+7 (34%)
303.79347	0.0145	H-3->L+6 (15%), H-2->L+7 (23%), H-1->L+6 (10%)
303.27331	0.0492	H-3->L+6 (13%), H-2->L+6 (30%), H-1->L+7 (12%)
303.21397	0.1112	H-6->L+2 (36%), H-6->L+3 (21%), H-1->L+7 (18%)
302.60713	0.068	H-6->L+3 (21%), H-2->L+7 (17%)
301.39338	0.028	H-6->L+3 (22%), H-3->L+6 (21%), H-2->L+7 (16%), H-1->L+6 (12%)

300.87409	0.0545	H-8->LUMO (17%), H-7->L+1 (17%), H-3->L+7 (15%)
300.55317	0.0624	H-7->L+1 (10%), H-3->L+7 (45%), H-2->L+6 (10%)
299.89888	0.018	H-8->L+1 (25%), H-7->LUMO (20%)

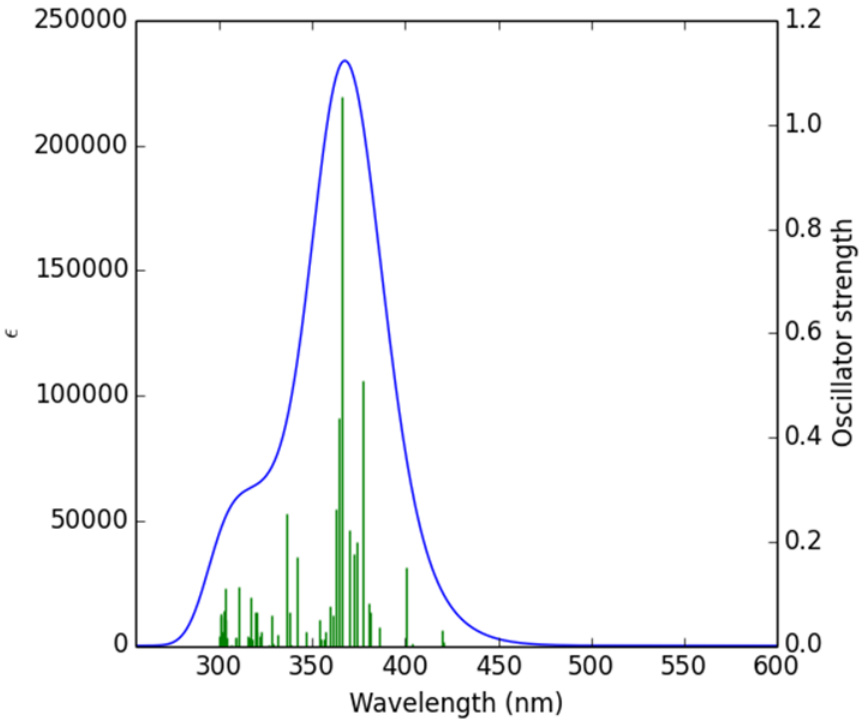

Figure S26. Calculated electronic absorption spectrum (B3LYP/6-31G(d,p)) of **1-H**.

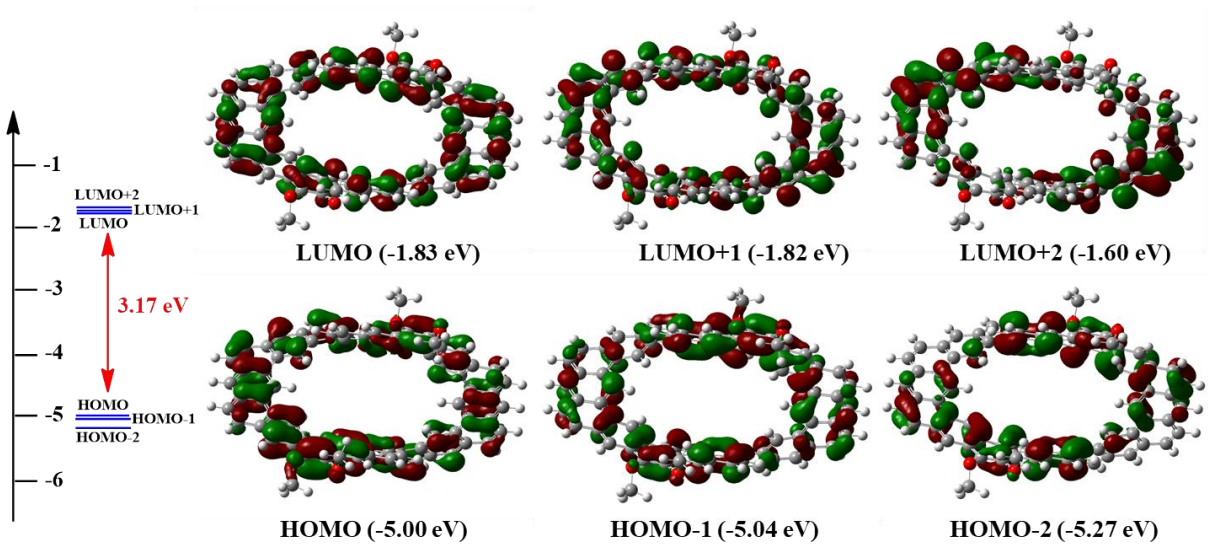

Figure S27. Frontier molecular orbital profiles and energy diagram of **1** obtained by B3LYP/6-31G(d,p) level calculation.

Table S2. Selected TD-DFT (B3LYP/6-31G(d,p)) calculated energies, oscillator strength and compositions of major electronic transitions of **1**.

Wavelength (nm)	Osc.Strength (f)	Major contributions
464.42985	0.0025	HOMO->LUMO (80%)
454.07139	0.0024	H-1->L+1 (79%)
446.53242	0.0518	H-1->LUMO (48%), HOMO->L+1 (44%)

438.75785	0.0177	H-3->LUMO (14%), H-2->L+1 (14%), H-1->LUMO (12%), HOMO->L+1 (16%), HOMO->L+2 (21%)
428.2701	0.0186	H-5->L+1 (15%), H-4->LUMO (21%), H-1->L+3 (18%), HOMO->L+4 (18%)
423.24091	0.2973	H-1->LUMO (36%), HOMO->L+1 (35%), HOMO->L+2 (12%)
416.41766	0.0236	H-3->L+1 (14%), H-2->LUMO (34%), H-1->L+2 (21%), HOMO->L+3 (15%)
412.97779	0.0024	H-5->LUMO (11%), H-2->LUMO (12%), H-1->L+4 (10%), HOMO->L+3 (34%)
402.03701	9E-4	H-2->LUMO (36%), H-1->L+2 (43%)
397.43619	0.0539	H-4->LUMO (31%), H-3->LUMO (10%), HOMO->L+2 (38%)
395.78686	0.618	H-3->LUMO (25%), H-1->L+3 (38%)
395.14355	0.1904	H-4->L+1 (31%), H-1->L+3 (10%)
393.83817	0.563	H-2->L+1 (61%)
391.24075	0.1005	H-3->L+1 (34%), HOMO->L+3 (14%)
389.76483	0.0357	H-4->LUMO (19%), H-3->LUMO (19%), HOMO->L+4 (47%)
388.82364	0.0131	H-4->L+1 (24%), HOMO->L+5 (49%)
386.62902	0.0061	H-2->L+3 (12%), H-1->L+4 (33%)
383.01008	0.0247	H-5->LUMO (14%), H-4->L+2 (10%), H-2->L+3 (17%), H-1->L+4 (23%)
381.72473	0.539	H-5->L+1 (22%), H-1->L+5 (55%)
380.56476	0.0291	H-5->LUMO (23%), H-3->L+1 (17%), H-1->L+4 (17%)
379.26094	0.6979	H-5->L+1 (40%), H-2->L+2 (15%), H-1->L+5 (10%)
378.55457	0.109	H-5->LUMO (27%), H-3->L+2 (20%), HOMO->L+5 (11%)
375.2094	1.2762	H-2->L+2 (52%), H-1->L+5 (13%)
371.4437	0.0461	H-5->L+3 (13%), H-4->L+2 (12%), H-4->L+4 (20%), H-3->L+4 (13%)
370.61097	0.0731	H-4->L+2 (10%), H-4->L+3 (51%), H-2->L+4 (11%)
368.92372	0.0457	H-3->L+3 (60%)
367.54571	0.0811	H-4->L+2 (21%), H-3->L+2 (30%), H-2->L+3 (25%)
365.36864	0.0312	H-5->L+2 (26%), H-2->L+4 (63%)
364.0277	0.0133	H-5->L+3 (21%), H-4->L+4 (11%), H-2->L+5 (43%)
362.87702	0.0333	H-5->L+2 (31%), H-3->L+5 (23%)
361.82861	0.0854	H-5->L+5 (16%), H-4->L+4 (15%), H-3->L+4 (22%), H-2->L+3 (11%), H-2->L+5 (12%)
352.56837	0.029	H-5->L+2 (13%), H-3->L+5 (56%)
349.44812	0.0079	H-4->L+5 (79%)
346.89626	0.0676	H-6->LUMO (19%), H-5->L+3 (11%), H-4->L+2 (10%), H-4->L+4 (16%), H-3->L+4 (22%)
345.44647	0.0285	H-5->L+4 (61%)
343.83703	0.1037	H-6->LUMO (17%), H-4->L+4 (11%), H-3->L+4 (16%), HOMO->L+6 (31%)
343.17084	0.0361	H-7->LUMO (14%), H-1->L+6 (27%), HOMO->L+7 (25%)
342.22361	0.0315	H-7->L+1 (10%), H-6->LUMO (11%), H-5->L+3 (14%), H-2->L+5 (12%), H-1->L+7 (16%), HOMO->L+6 (16%)
341.65778	0.0499	H-7->LUMO (27%), H-6->L+1 (26%), H-1->L+6 (17%), HOMO->L+7 (24%)
339.1067	0.0081	H-6->L+1 (46%)
338.47719	0.1287	H-6->LUMO (16%), H-5->L+5 (49%), HOMO->L+6 (12%)
336.16451	0.0072	H-7->LUMO (15%), H-7->L+1 (14%), H-1->L+6 (18%), H-1->L+7 (23%)
336.05517	0.005	H-7->LUMO (18%), H-1->L+6 (12%), H-1->L+7 (29%)
333.14755	0.1153	H-7->L+1 (46%), HOMO->L+6 (16%)
332.31712	0.0126	H-7->L+3 (11%), H-6->L+2 (24%), H-2->L+7 (16%)
329.57865	0.0108	H-6->L+4 (18%), H-5->L+7 (12%), H-4->L+6 (13%), H-3->L+6 (10%)
325.80264	0.0066	H-8->L+1 (15%), H-6->L+3 (34%), H-2->L+6 (13%)
322.41371	0.0344	H-8->L+1 (22%), HOMO->L+8 (37%)
321.38575	0.0044	H-7->L+3 (26%), H-6->L+2 (31%), H-3->L+6 (12%)
321.22754	7E-4	H-8->LUMO (39%), H-1->L+8 (22%)

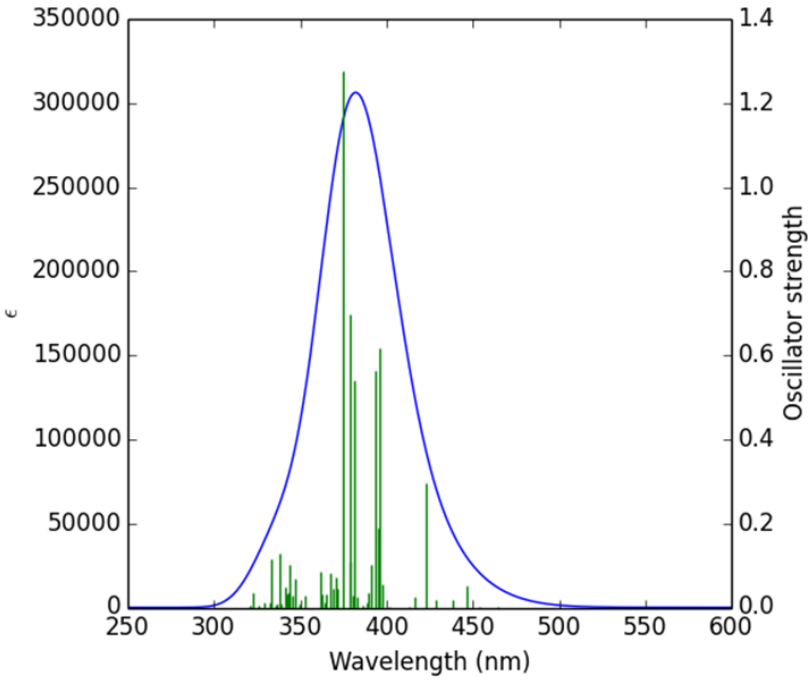

Figure S28. Calculated electronic absorption spectrum (B3LYP/6-31G(d,p)) of **1**.

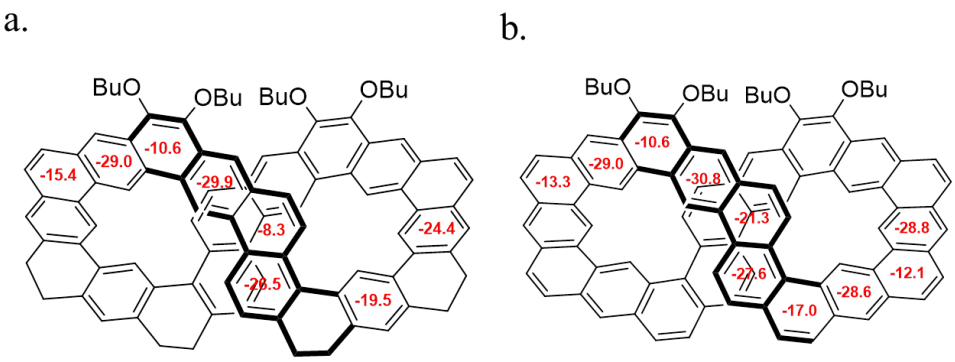

Figure S29. Calculated NICS(1)$_{zz}$ values (ppm) of (a) **1-H** and (b) **1**.

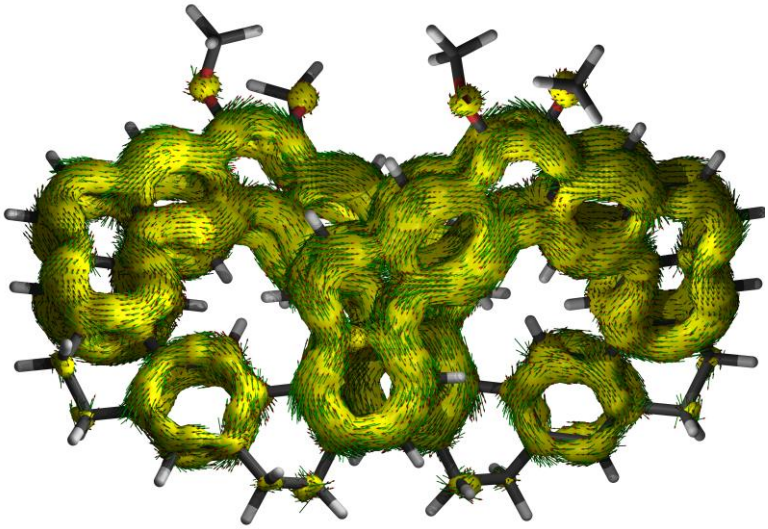

Figure S30. Calculated ACID plots of **1-H** with isovalue of 0.02. The magnetic field is pointing in through the paper.

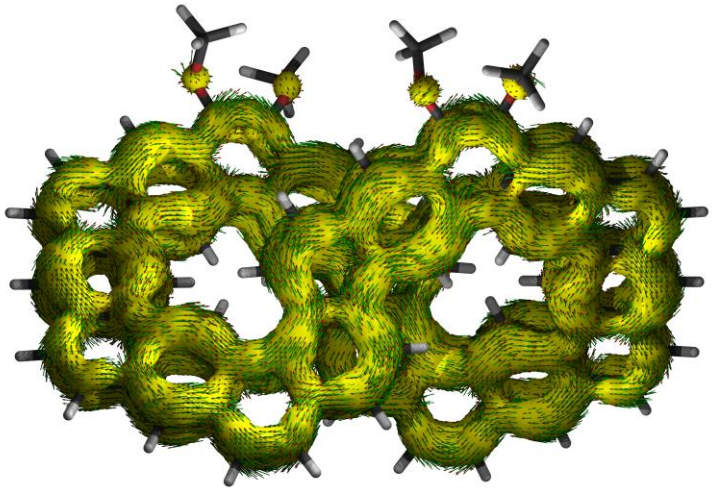

Figure S31. Calculated ACID plots of **1** with isovalue of 0.02. The magnetic field is pointing in through the paper.

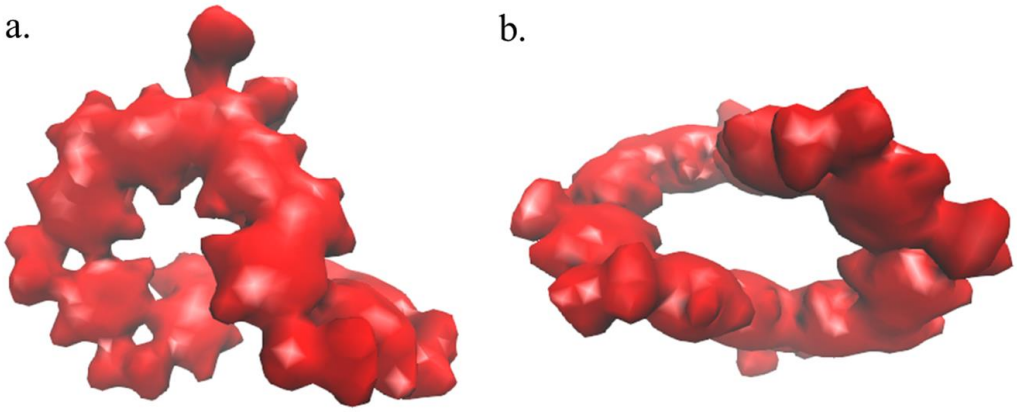

Figure S32. Calculated 3D ICSS maps of **1-H** with isovalue of 6 (left for side-view and right for top-view).

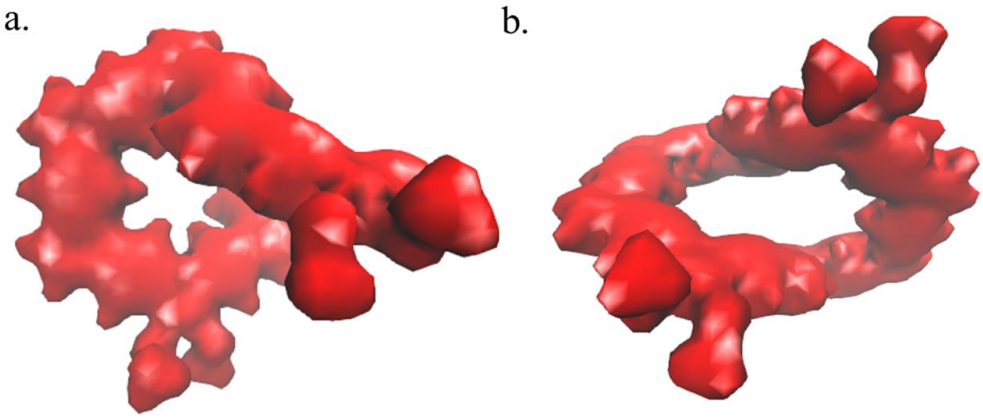

Figure S33. Calculated 3D ICSS maps of **1** with isovalue of 6 (left for side-view and right for top-view).

5. X-ray crystallographic data for 1-H

Crystallographic data have been deposited with the Cambridge Crystallographic Data Centre as supplementary publication no. CCDC 2099885 for **1-H**. The X-ray intensity data were measured at low temperature (T=100K), using a four circles goniometer Kappa geometry, Bruker AXS D8 Venture, equipped with a Photon 100 CMOS active pixel sensor detector. Frames were integrated with the Bruker SAINT8 software package. Data were corrected for absorption effects using the multi-scan method (SADABS).[9] Molecule was solved with the software SHELXT,[10] using a Dual Space method. Refinement of the structure was performed by least squares procedures on weighted F2 values using the SHELXL-version 2014/6[11] included in the WinGx system programs for Windows.[12] The crystallographic data were summarized in Table S3.

Table S3. Crystallographic data of **1-H**.

	1-H
Chemical formula	$C_{98}H_{84}Cl_4O_4$
Formula weight	1476.45
Crystal system	monoclinic
Space group	-P 2yn
Calculated density	1.345 Mg/m^3
a (Å)	15.1951(5)
b (Å)	22.9211(8)
c (Å)	21.1399(7)
α (°)	90
β(°)	100.292(2)
γ (°)	90
Unit cell volume ($Å^3$)	7244.3(4)
Temperature (K)	100(2)
No. of formula units per unit cell	4
No. of reflections measured	12746
No. of independent reflections	10416
Rint	0.1049
Final R1 [I>2sigma(I)]	0.0919

6. NMR spectra and HR-mass spectra for all new compounds

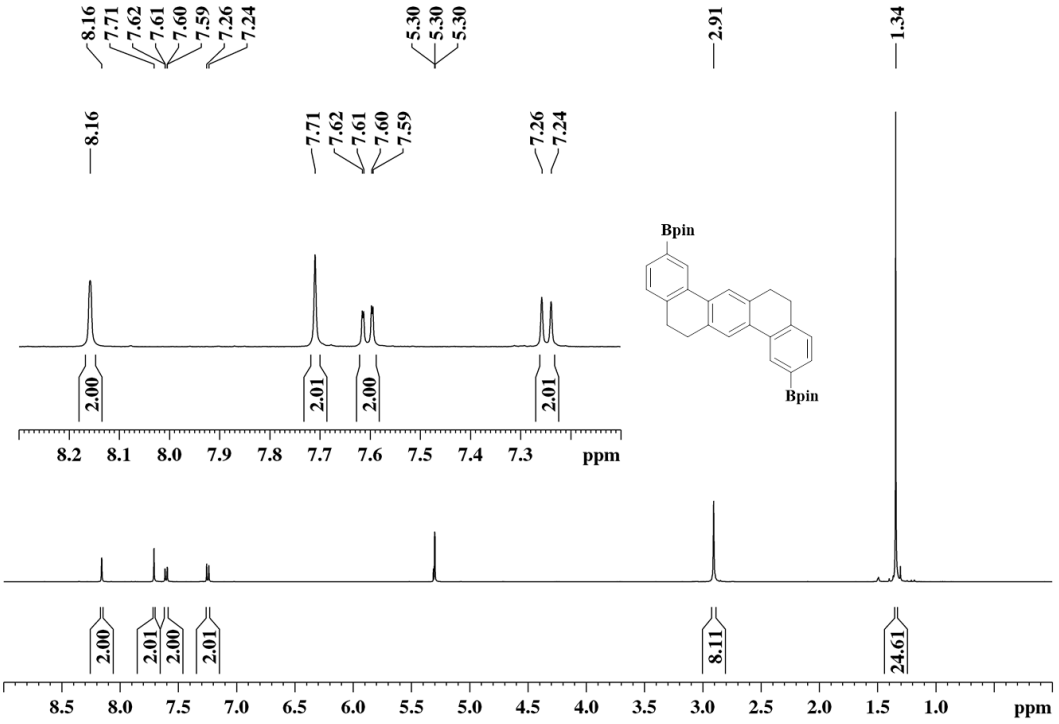

Figure S34. ^{1}H NMR spectrum of **5'** in CD_2Cl_2 (400 MHz, 298 K)

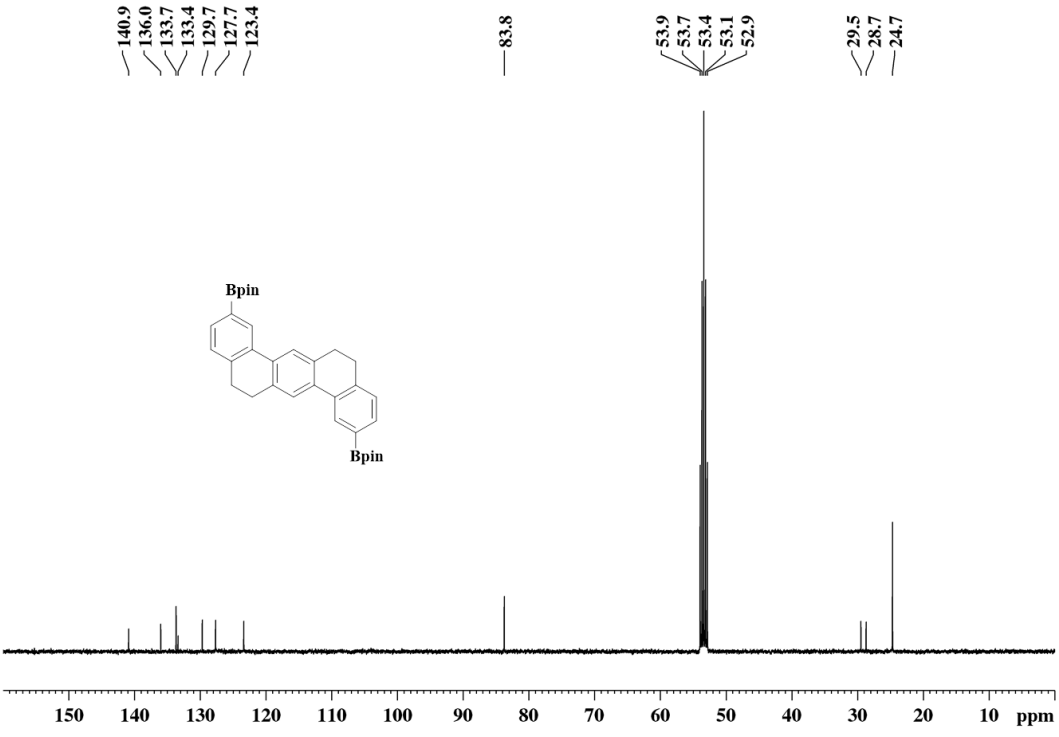

Figure S35. ^{13}C NMR spectrum of **5'** in CD_2Cl_2 (100 MHz, 298 K)

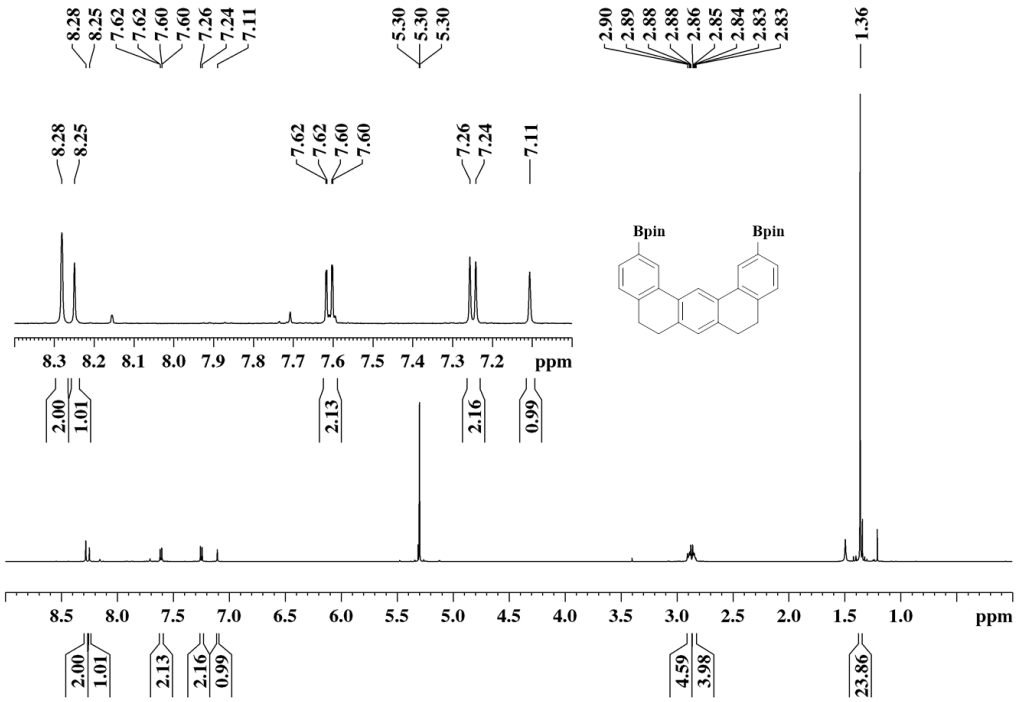

Figure S36. ^{1}H NMR spectrum of **5** in CD_2Cl_2 (400 MHz, 298 K)

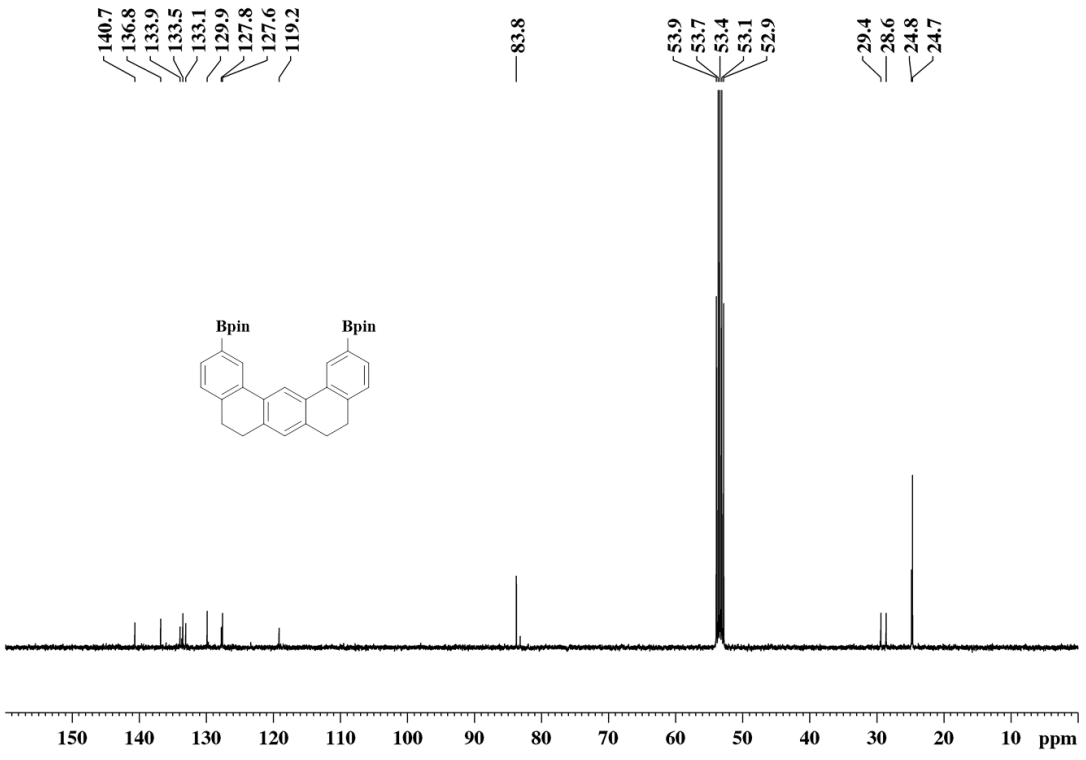

Figure S37. ^{13}C NMR spectrum of **5** in CD_2Cl_2 (100 MHz, 298 K)

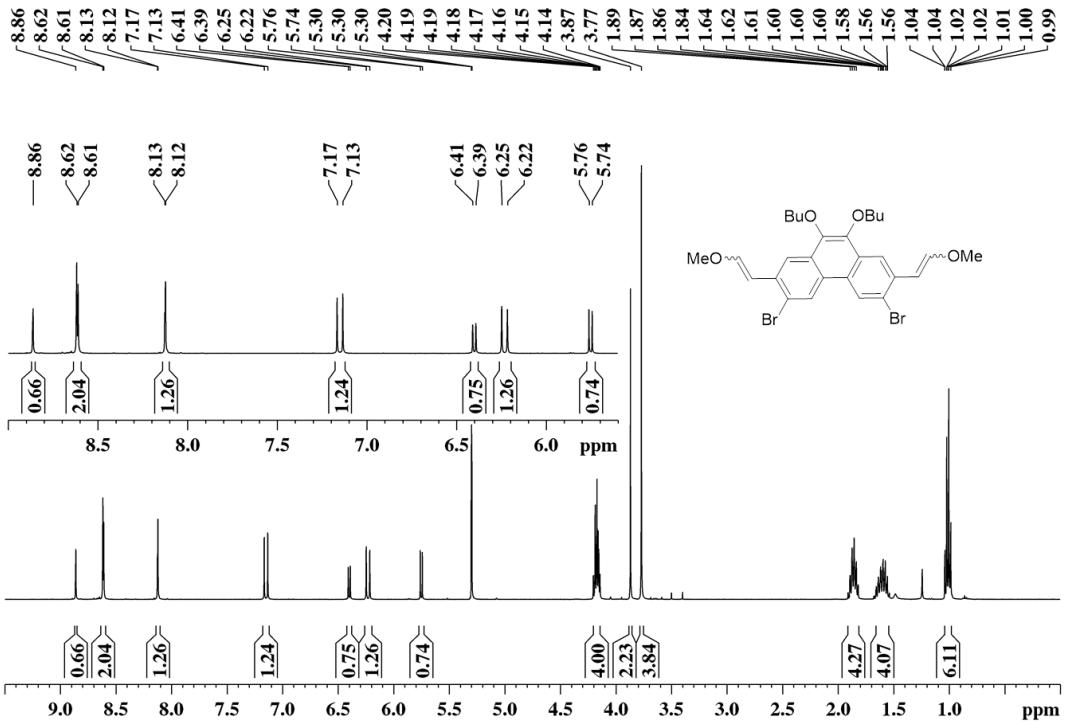

Figure S38. ^{1}H NMR spectrum of **6** in CD_2Cl_2 (400 MHz, 298 K)

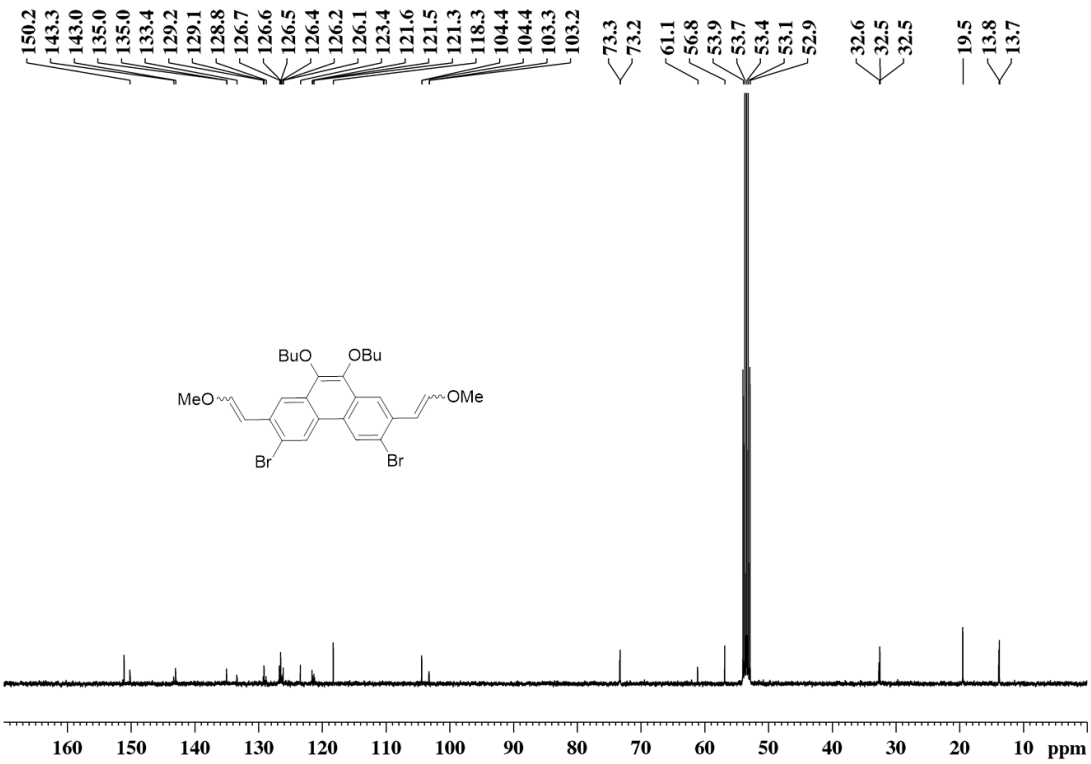

Figure S39. ^{13}C NMR spectrum of **6** in CD_2Cl_2 (100 MHz, 298 K)

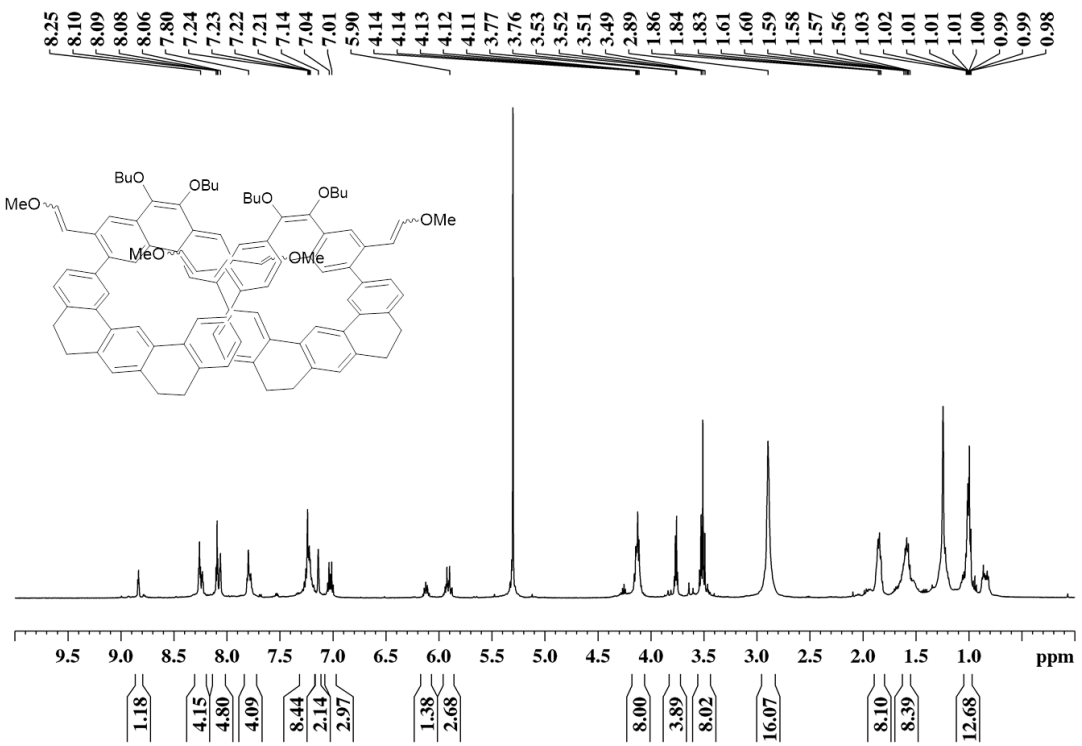

Figure S40. ^{1}H NMR spectrum of **7** in CD_2Cl_2 (400 MHz, 298 K)

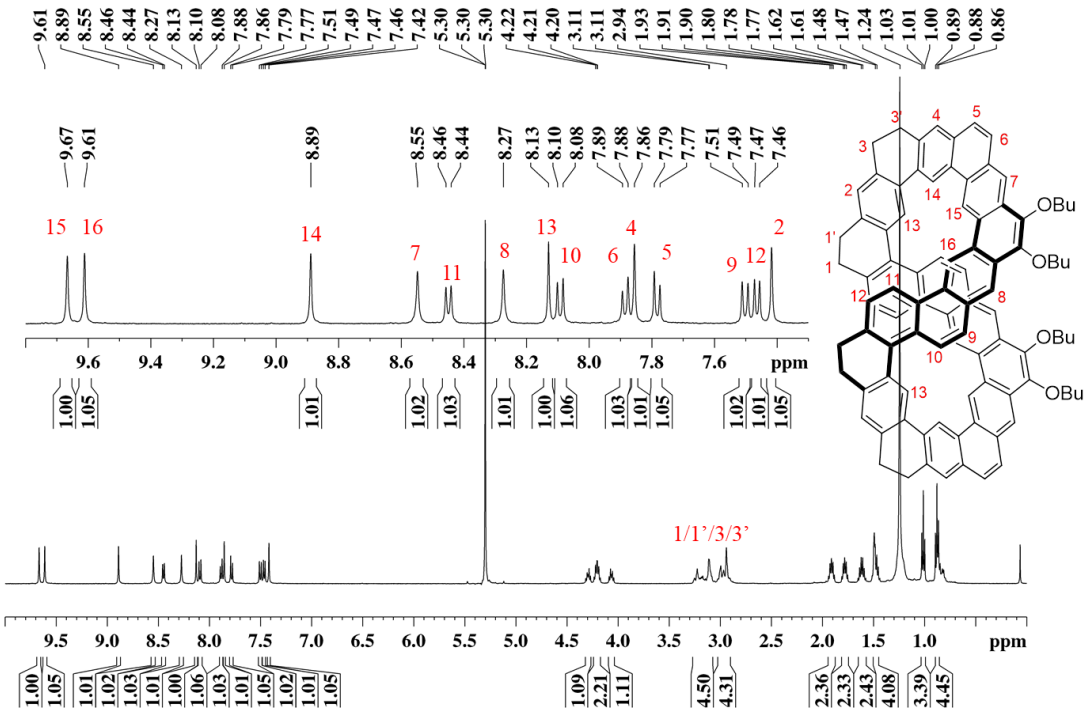

Figure S41. ^{1}H NMR spectrum of **1-H** in CD_2Cl_2 (500 MHz, 298 K)

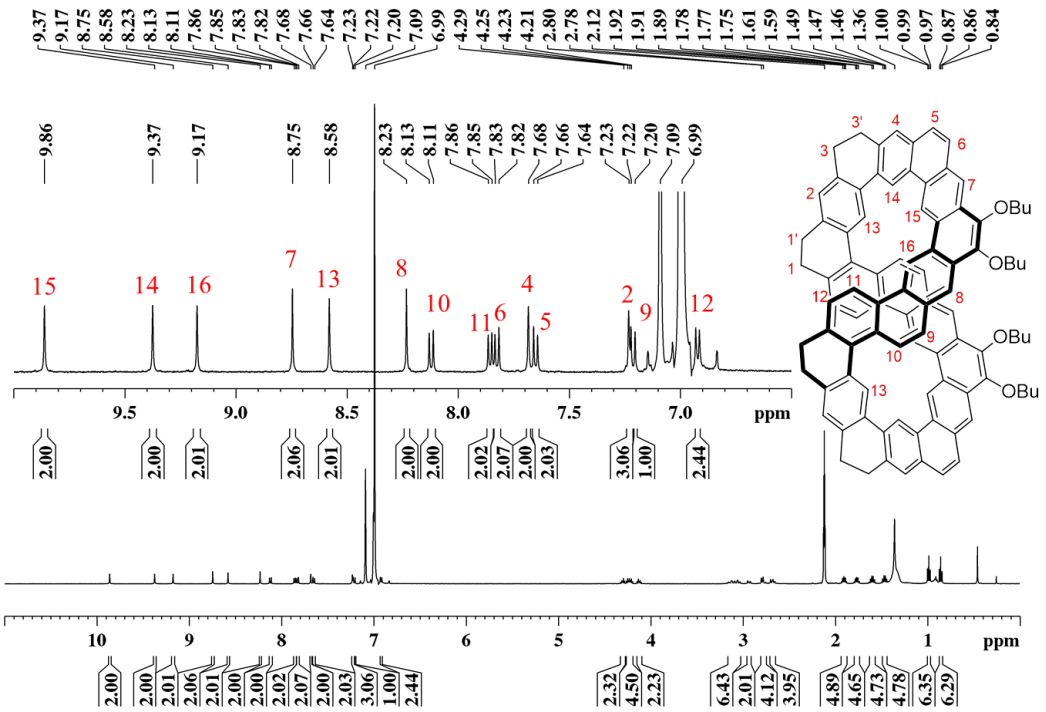

Figure S42. ^{1}H NMR spectrum of **1-H** in Toluene-d_8 (500 MHz, 373 K)

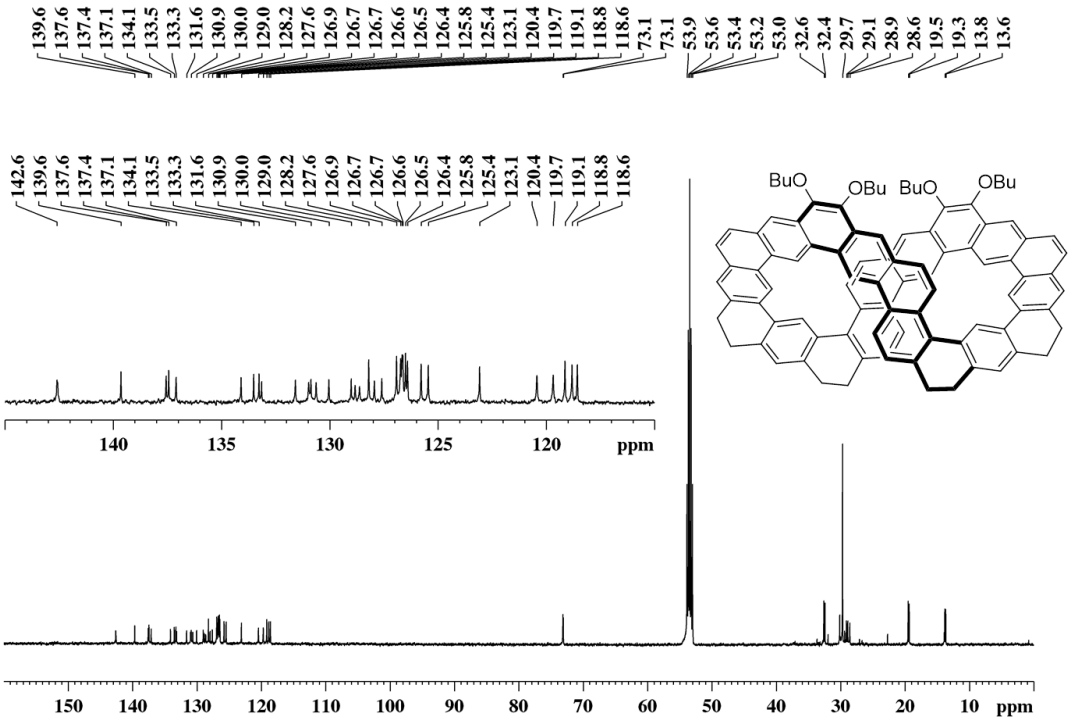

Figure S43. ^{13}C NMR spectrum of **1-H** in $CDCl_2$ (125 MHz, 298 K)

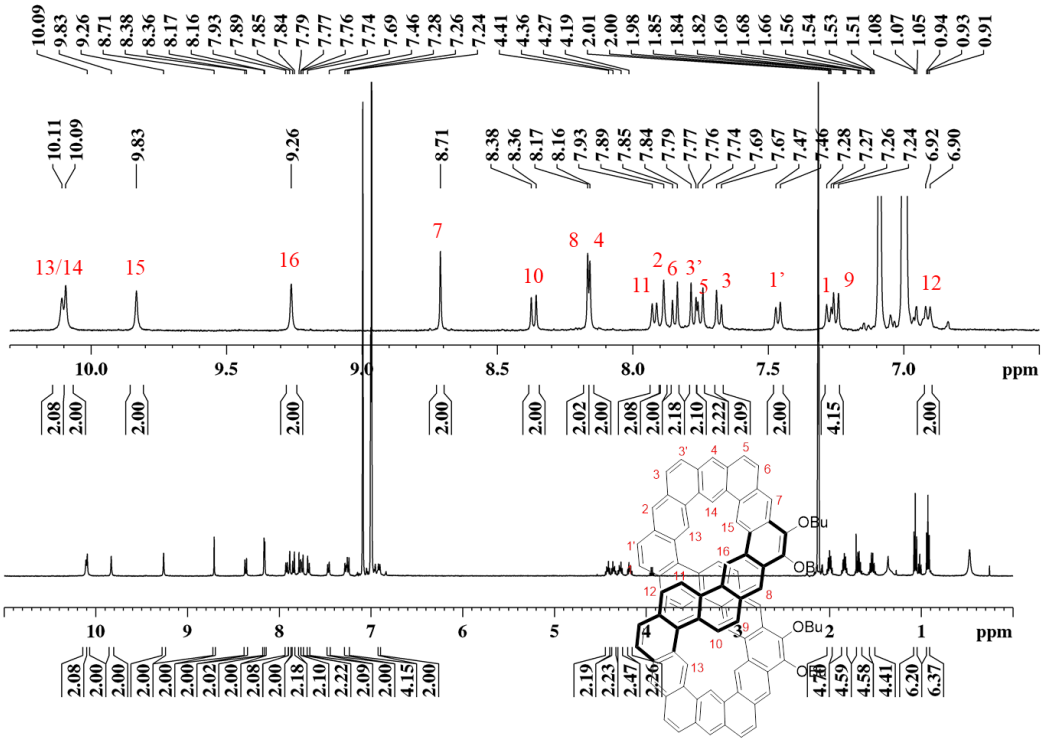

Figure S44. ^{1}H NMR spectrum of **1** in Toluene-d_8 (500 MHz, 373 K)

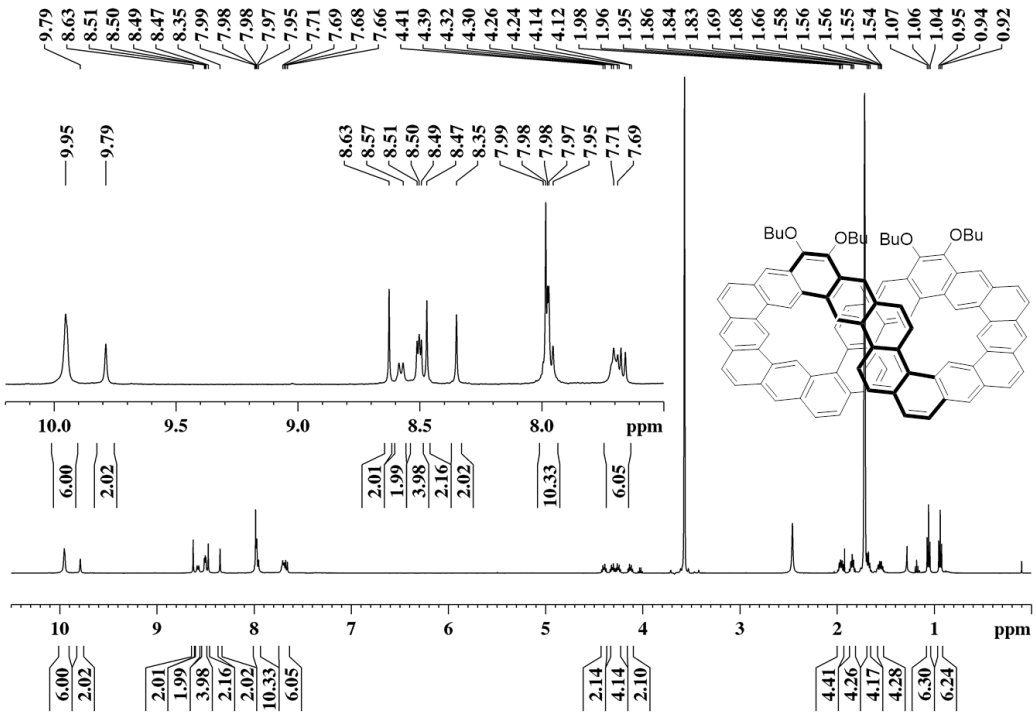

Figure S45. ^{1}H NMR spectrum of **1** in THF-d_8 (500 MHz, 298 K)

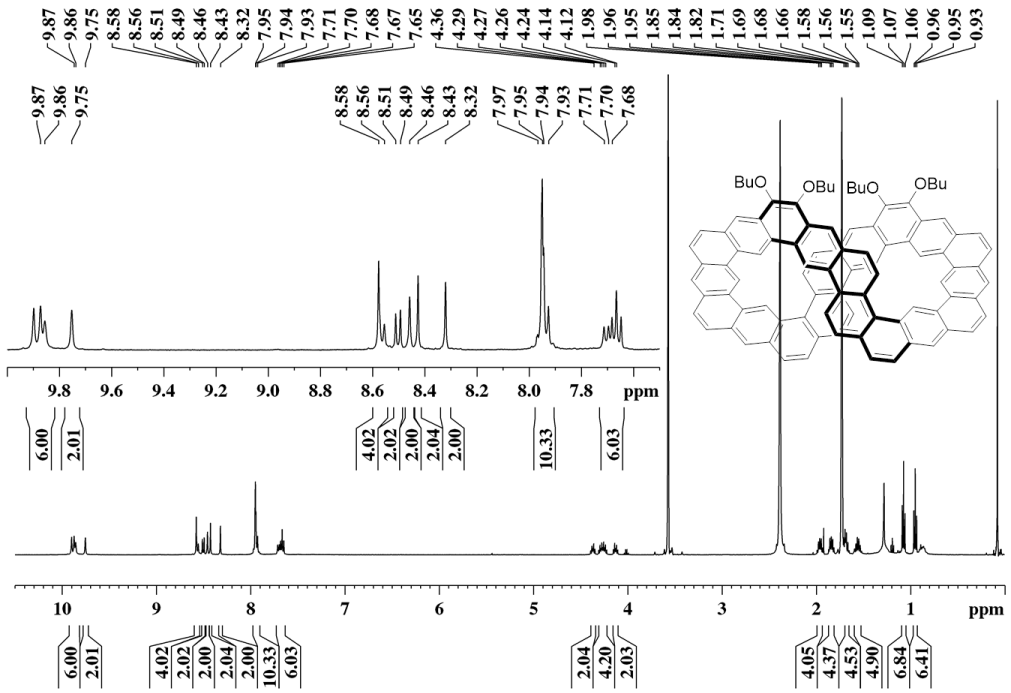

Figure S46. ^{1}H NMR spectrum of **1** in THF-d_8:CS_2 = 2:1 (500 MHz, 298 K)

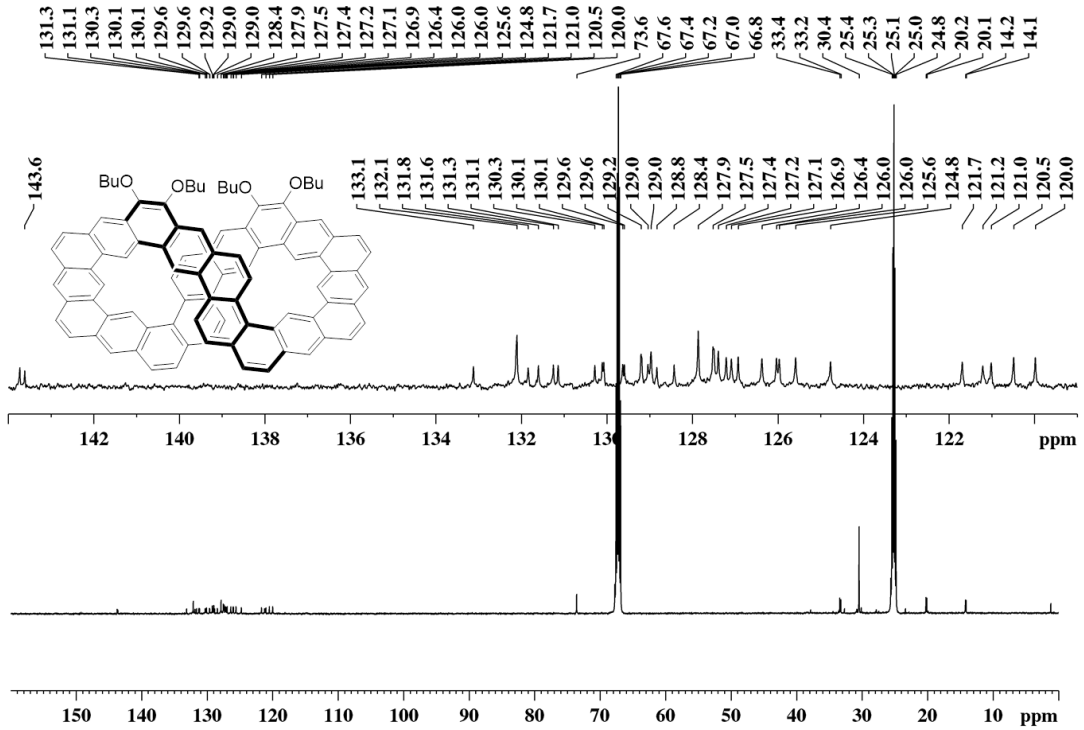

Figure S47. ^{13}C NMR spectrum of **1** in Toluene-d_8 (500 MHz, 298 K)

MALDI,2,20210622

Analysis Info

Analysis Name	D:\Data\MALDI\2021\0624\2_0_C3_000001.d	Acquisition Date	6/24/2021 6:15:22 PM
Method	MALDI_P_100-3000	Operator	
Sample Name	MURU-N-ESI	Instrument	solariX
Comment			

Acquisition Parameter

Acquisition Mode	Single MS	Acquired Scans	2	Calibration Date	Thu Jun 24 06:06:37
Polarity	Positive	No. of Cell Fills	1	Data Acquisition Size	2097152
Broadband Low Mass	202.1 m/z	No. of Laser Shots	10	Data Processing Size	4194304
Broadband High Mass	1000.0 m/z	Laser Power	55.4 lp	Apodization	Sine-Bell Multiplication
Source Accumulation	0.001 sec	Laser Shot Frequency	0.020 sec		
Ion Accumulation Time	0.100 sec				

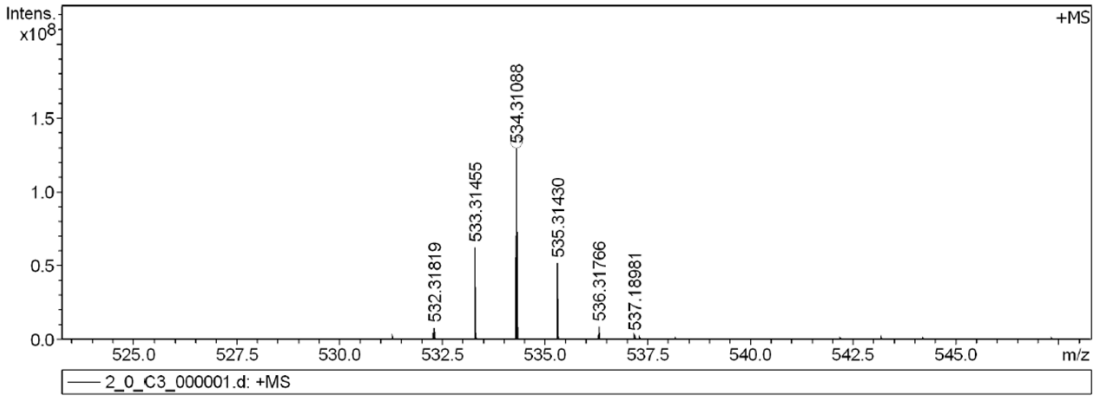

Meas. m/z	#	Ion Formula	Score	m/z	err [ppm]	Mean err [ppm]	mSigma	rdb	e⁻ Conf	N-Rule
534.310885	1	C34H40B2O4	100.00	534.311873	-0.3	1.1	30.7	16.0	odd	ok

Figure S48. HR mass spectrum (MALDI-TOF) of **5**

MALDI,3,20210622

Analysis Info

Analysis Name	D:\Data\MALDI\2021\0624\3_0_C4_000003.d	Acquisition Date	6/24/2021 6:18:17 PM
Method	MALDI_P_100-3000	Operator	
Sample Name	MURU-N-ESI	Instrument	solariX
Comment			

Acquisition Parameter

Acquisition Mode	Single MS	Acquired Scans	2	Calibration Date	Thu Jun 24 06:06:37
Polarity	Positive	No. of Cell Fills	1	Data Acquisition Size	2097152
Broadband Low Mass	202.1 m/z	No. of Laser Shots	10	Data Processing Size	4194304
Broadband High Mass	1000.0 m/z	Laser Power	48.6 lp	Apodization	Sine-Bell Multiplication
Source Accumulation	0.001 sec	Laser Shot Frequency	0.020 sec		
Ion Accumulation Time	0.100 sec				

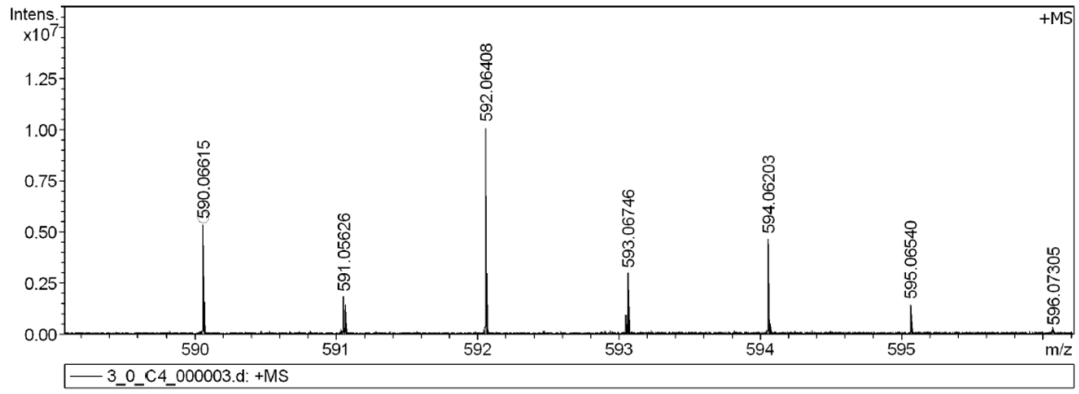

Meas. m/z	#	Ion Formula	Score	m/z	err [ppm]	Mean err [ppm]	mSigma	rdb	e⁻ Conf	N-Rule
590.066147	1	C28H32Br2O4	100.00	590.066185	-0.1	0.5	28.1	12.0	odd	ok

Figure S49. HR mass spectrum (MALDI-TOF) of **6**

MALDI,4,20210622

Analysis Info

Analysis Name	D:\Data\MALDI\2021\0624\4_0_C5_000003.d	Acquisition Date	6/24/2021 6:20:56 PM
Method	MALDI_P_100-3000	Operator	
Sample Name	MURU-N-ESI	Instrument	solariX
Comment			

Acquisition Parameter

Acquisition Mode	Single MS	Acquired Scans	3	Calibration Date	Thu Jun 24 06:06:37
Polarity	Positive	No. of Cell Fills	1	Data Acquisition Size	2097152
Broadband Low Mass	202.1 m/z	No. of Laser Shots	20	Data Processing Size	4194304
Broadband High Mass	2600.0 m/z	Laser Power	52.6 lp	Apodization	Sine-Bell Multiplication
Source Accumulation	0.001 sec	Laser Shot Frequency	0.020 sec		
Ion Accumulation Time	0.100 sec				

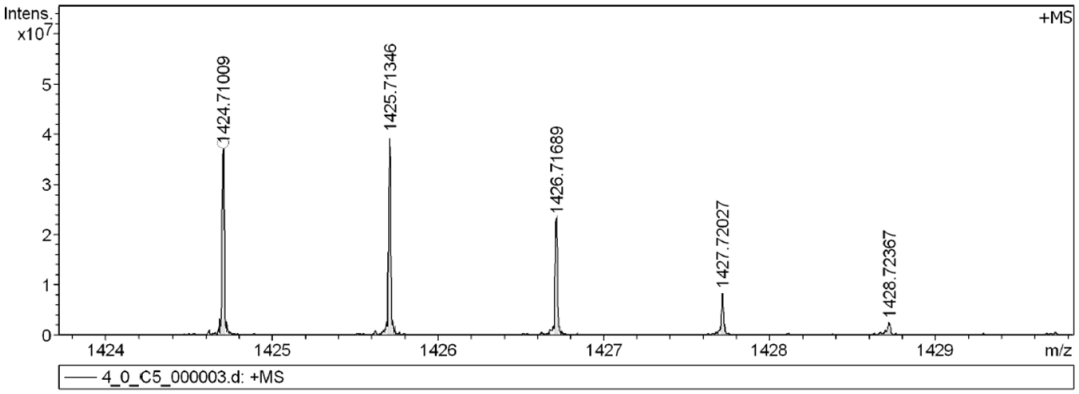

Meas. m/z	#	Ion Formula	Score	m/z	err [ppm]	Mean err [ppm]	mSigma	rdb	e⁻ Conf	N-Rule
1424.710088	1	C100H96O8	100.00	1424.709971	0.1	-0.1	14.5	53.0	odd	ok

Figure S50. HR mass spectrum (MALDI-TOF) of **7**

MALDI,5,20210622

Analysis Info

Analysis Name	D:\Data\MALDI\2021\0624\5_0_C6_000003.d	Acquisition Date	6/24/2021 6:23:53 PM
Method	MALDI_P_100-3000	Operator	
Sample Name	MURU-N-ESI	Instrument	solariX
Comment			

Acquisition Parameter

Acquisition Mode	Single MS	Acquired Scans	2	Calibration Date	Thu Jun 24 06:06:37
Polarity	Positive	No. of Cell Fills	1	Data Acquisition Size	2097152
Broadband Low Mass	202.1 m/z	No. of Laser Shots	30	Data Processing Size	4194304
Broadband High Mass	2400.0 m/z	Laser Power	52.6 lp	Apodization	Sine-Bell Multiplication
Source Accumulation	0.001 sec	Laser Shot Frequency	0.020 sec		
Ion Accumulation Time	0.100 sec				

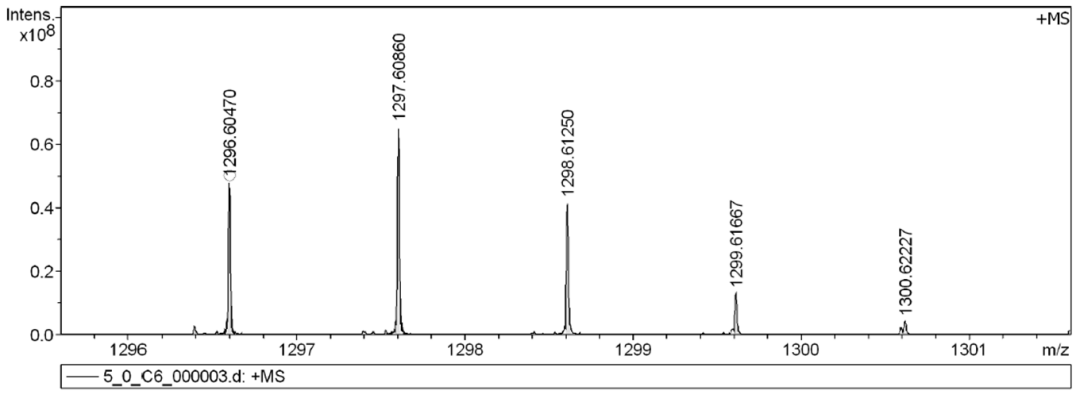

Meas. m/z	#	Ion Formula	Score	m/z	err [ppm]	Mean err [ppm]	mSigma	rdb	e⁻ Conf	N-Rule
1296.604698	1	C96H80O4	100.00	1296.605112	0.3	-0.2	100.5	57.0	odd	ok

Figure S51. HR mass spectrum (MALDI-TOF) of **1-H**

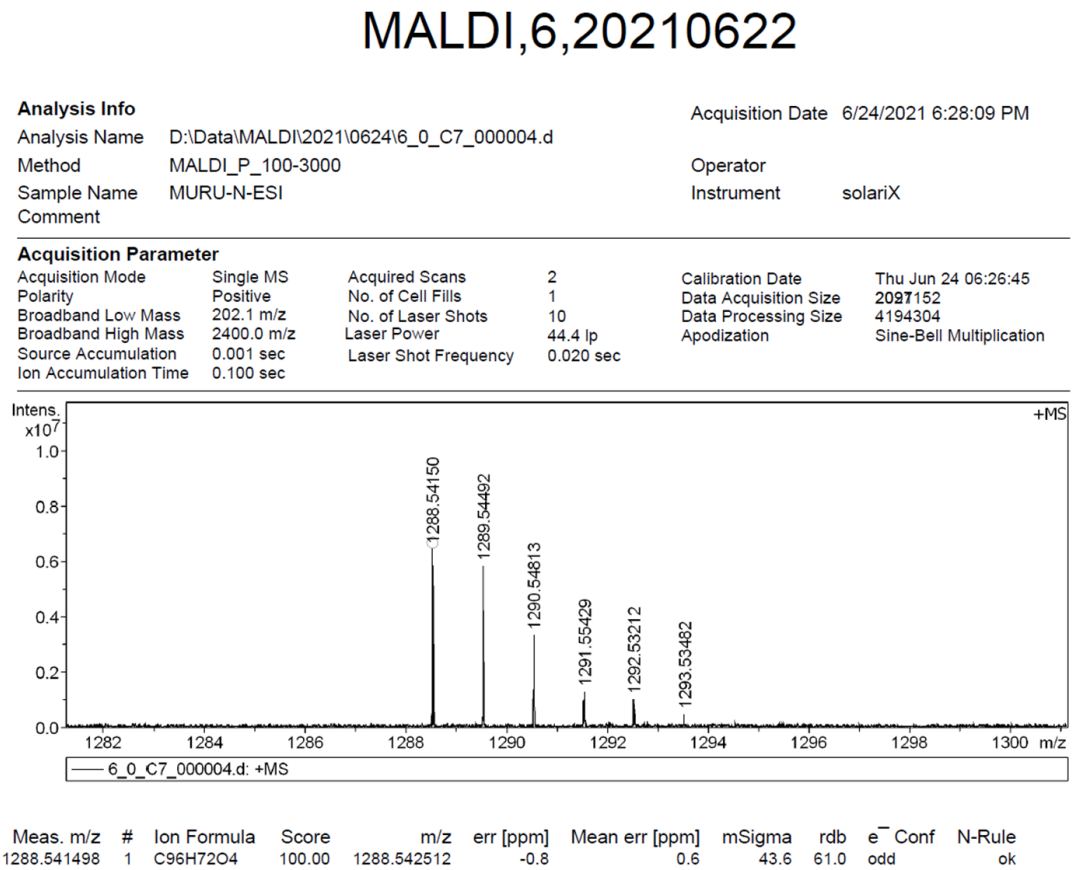

Figure S52. HR mass spectrum (MALDI-TOF) of **1**

7. References

(1) Suzuki, S.; Itami, K.; Yamaguchi, J. Synthesis of Octaaryl Naphthalenes and Anthracenes with Different Substituents. *Angew.Chem.Int. Ed.* **2017**, *56*,15010.

(2) Gregolińska, H.; Majewski, M.; Chmielewski, P. J.; Gregoliński, J.; Chien, A.; Zhou, J.; Wu, Y. L.; Bae, Y. J.; Wasielewski, M. R.; Zimmerman, P. M.; Stępień, M. Fully Conjugated [4]Chrysaorene. Redox-Coupled Anion Binding in a Tetraradicaloid Macrocycle *J. Am. Chem. Soc.* **2018**, *140*, 14474.

(3) *Gaussian 09; Revision A.2*; Frisch, M. J.; Trucks, G. W.; Schlegel, H. B.; Scuseria, G. E.; Robb, M. A.; Cheeseman, J. R.; Scalmani, G.; Barone, V.; Mennucci, B.; Petersson, G. A.; Nakatsuji, H.; Caricato, M.; Li, X.; Hratchian, H. P.; Izmaylov, A. F.; Bloino, J.; Zheng, G.; Sonnenberg, J. L.; Hada, M.; Ehara, M.; Toyota, K.; Fukuda, R.; Hasegawa, J.; Ishida, M.; Nakajima, T.; Honda, Y.; Kitao, O.; Nakai, H.; Vreven, T.; Montgomery, J., J. A.; Peralta, J. E.; Ogliaro, F.; Bearpark, M.; Heyd, J. J.; Brothers, E.; Kudin, K. N.; Staroverov, V. N.; Kobayashi, R.; Normand, J.; Raghavachari, K.; Rendell, A.; Burant, J. C.; Iyengar, S. S.; Tomasi, J.; Cossi, M.; Rega, N.; Millam, N. J.; Klene, M.; Knox, J. E.; Cross, J. B.; Bakken, V.; Adamo, C.; Jaramillo, J.; Gomperts, R.; Stratmann, R. E.; Yazyev, O.; Austin, A. J.; Cammi, R.; Pomelli, C.; Ochterski, J. W.; Martin, R. L.; Morokuma, K.; Zakrzewski, V. G.; Voth, G. A.; Salvador, P.; Dannenberg, J. J.; Dapprich, S.; Daniels, A. D.; Farkas, Ö.; Foresman, J. B.; Ortiz, J. V.;

Cioslowski, J.; Fox, D. J.; Gaussian, Inc., Wallingford CT, **2009**.

(4) (a) Becke, A. D. Density-functional thermochemistry. III. The role of exact exchange. *J. Chem. Phys.* **1993**, *98*, 5648. (b) Lee, C.; Yang, W.; Parr, R. G. Development of the Colle-Salvetti Correlation-energy Formula into a Functional of the Electron Density. *Phys. Rev. B: Condens. Matter* **1988**, *37*, 785. (c) Yanai, T.; Tew, D.; Handy, N. A New Hybrid Exchange-correlation Functional Using the Coulomb-attenuating Method (CAM-B3LYP). *Chem. Phys. Lett.* **2004**, *393*, 51. (d) Ditchfield, R.; J. Hehre, W.; Pople, J. A. Self-Consistent Molecular-Orbital Methods. IX. An Extended Gaussian-Type Basis for Molecular-Orbital Studies of Organic Molecules. *J. Chem. Phys.* **1971**, *54*, 724. (e) Hehre, W. J.; Ditchfield, R.; Pople, J. A. Self-Consistent Molecular Orbital Methods. XII. Further Extensions of Gaussian-Type Basis Sets for Use in Molecular Orbital Studies of Organic Molecules. *J. Chem. Phys.* **1972**, *56*, 2257. (f) Hariharan, P. C.; Pople, J. A. The Influence of Polarization Functions on Molecular Orbital Hydrogenation Energies. *Theor. Chim. Acta* **1973**, *28*, 213.

(5) Schleyer, P. v. R.; Maerker, C.; Dransfeld, A.; Jiao, H. J.; Hommes, N. J. R. v. E. Nucleus-Independent Chemical Shifts: A Simple and Efficient Aromaticity Probe. *J. Am. Chem. Soc.* **1996**, *118*, 6317.

(6) Geuenich, D.; Hess, K.; Köhler, F.; Herges, R. Anisotropy of the Induced Current Density (ACID), a General Method to Quantify and Visualize Electronic Delocalization. *Chem. Rev.* **2005**, *105*, 3758.

(7) Lu, T.; Chen, F. Multiwfn: A multifunctional wavefunction analyzer. *J. Comput. Chem.* **2012**, *33*, 580.

(8) Humphrey, W.; Dalke, A.; Schulten, K. VMD: Visual Molecular Dynamics. *J. Mol. Graph.* **1996**, *14*, 33.

(9) SADABS. Ver. 2014/5. Krause, L., Herbs-Irmer, R., Sheldrick, G. M. Stalke, D. (2015). *J. Appl. Crystallogr.* 48.

(10) SHELXT-Integrated space-group and crystal-structure determination Sheldrick, G. M. *Acta Crystallogr., Sect. A* **2015**, A71, 3.

(11) SHELXTL G. M. Sheldrick, Ver. 2014/7. *Acta Crystallographica. Sect C Structural Chemistry* 71, 3.

(12) Farrugia, L. J. *WinGX* suite for small-molecule single-crystal crystallography. *J. Appl. Cryst*. **1999**, *32*, 837.